Hot-wire Measurements in a Three-Dimensional Turbulent Corner Wall Jet

by

Barrett J. Poole

Bachelor's of Science in Engineering, 2009

A Thesis Submitted in Partial Fulfillment of the Requirements for the Degree of

Master's of Science in Engineering

In the Graduate Academic Unit of Mechanical Engineering

Supervisor(s):	Joseph Hall, Ph.D, Mechanical Engineering
Examining Board:	Andy Simoneau, Ph.D, Mechanical Engineering, Chair
	Andrew Gerber, Ph.D, Mechanical Engineering
	Brian Lowry, Ph.D, Chemical Engineering

This thesis is accepted by the
Dean of Graduate Studies

The University of New Brunswick

February 2014

.

Abstract

When a jet of fluid is ejected parallel to a flat surface from a nozzle the fluid has a tendency to stick to the surface and spread more rapidly in the lateral direction than normal to the wall, as the jet evolves downstream. In order to improve our understanding of the jet, several researchers have altered many aspects of the jet and studied the resulting flow. The corner wall jet (one such alteration) is similar to the standard three-dimensional wall jet with the exception that one half of the surface has been rotated counter-clockwise by 90° degrees. This same spreading behavior is also expected to occur in the corner jet; however, the extent of which is not fully understood. Turbulence measurements were performed in both the three-dimensional and corner wall jet to help understand the differences between these two flows.

Contents

List of Tables

List of Figures

Chapter 1

Introduction

When a jet of fluid is ejected parallel to a flat surface from a nozzle the fluid has a tendency to stick to the surface and thus spreads faster laterally than normal to the wall. This flow is known as a wall jet and is shown in figure 1.1. The flow near the surface behaves somewhat like a turbulent boundary-layer, while the flow above that layer acts like that of a free jet. The three-dimensional wall jet has been extensively studied in the past by many authors [2, 7, 8, 9, 10, 11]. Wall jets are used in practical applications such as cooling along the surface of a turbine blade or the inside of a combustion system. Wall jets are often integral to heating and ventilation systems and can also be used for controlling air contaminants in industrial environments.

The most interesting feature of the three-dimensional wall jet is that, for the turbulent case, the growth of the lateral half-width is 5 to 8 times larger than the growth of the jet vertically, normal to the wall. It is known that this disparity is not present for laminar 3D wall jets[12]. Whether or not the same behavior occurs in a turbulent corner wall jet (figure 1.2) is unclear and is the focus of this work. The corner wall jet is similar to a standard three-dimensional wall jet with the exception that one half of the surface has been rotated counter clockwise by 90° and the jet nozzle has been repositioned so that the center is as close to the corner as possible.

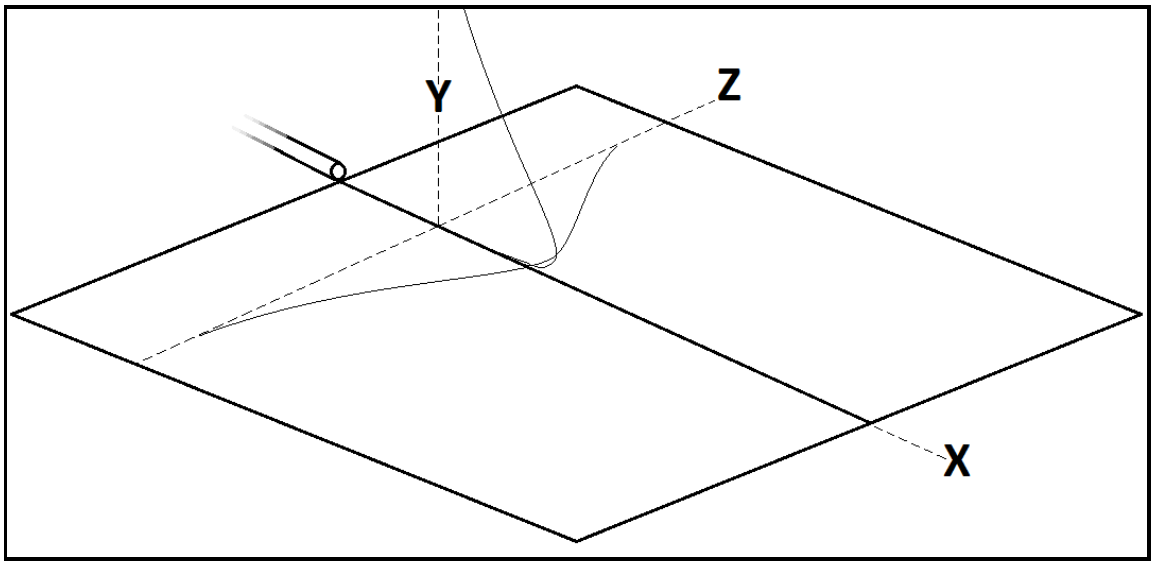

Figure 1.1: Schematic of a three-dimensional wall jet issuing from a round pipe.

In particular, the goal of this study is to improve our understanding of how the jet flow is altered by the corner in relation to the flat wall in the jet. In the past, there has been only one study on the corner wall jet, Hogg and Launder [6].

This thesis is outlined as follows: Chapter 2 presents a review of the literature relevant to the topic of wall jets and corner wall jets, Chapter 3, is a description of the experimental facilities and techniques, Chapter 4 discusses the results of this study, and the conclusions, and future work is discussed in Chapter 5.

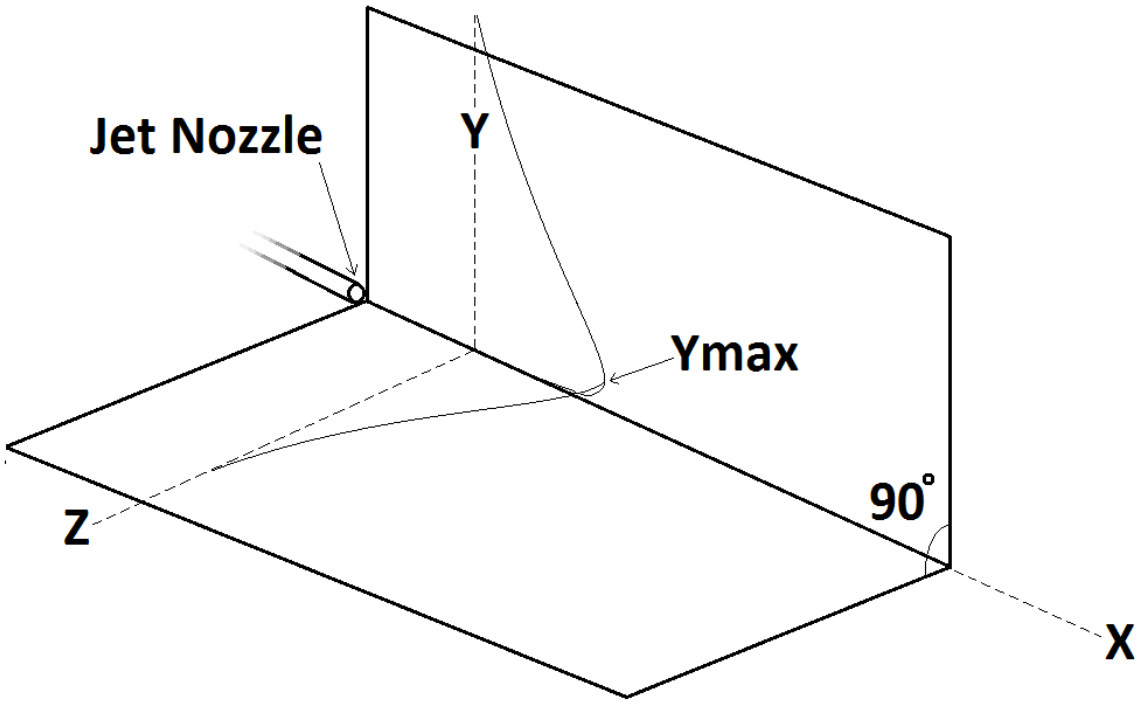

Figure 1.2: Schematic of a three-dimensional corner wall jet issuing fluid from a round pipe.

Chapter 2

Literature Review

2.1 Three-Dimensional Wall Jets

There have been a number of investigations of the turbulent three-dimensional wall jet, all of which have reported the large lateral growth of the flow [1, 2, 3, 4, 5, 6, 10, 9, 13]. Some of these early investigations include a three-dimensional wall jet issuing from a rectangular, sharp-edged orifice by Viets and Sforza [7], a jet exiting a long pipe by Newman et al [14] and studies done on flows exiting from a variety of different nozzle geometries by Rajaratnam et al [8] and Padmanabham and Gowda [15]. Padmanabham and Gowda varied the geometry of their nozzle by partially covering the nozzle with the wall at different ratio's of $\frac{h}{d}$ (0.8, 0.5, 0.23), as shown below in figure 2.1.

The development of the three-dimensional wall jet is typically characterized by inspecting the decay of the local maximum streamwise velocity and the variation of the vertical and lateral half-widths, $y_{\frac{1}{2}}$ and $z_{\frac{1}{2}}$, respectively. In the three-dimensional wall jet, the vertical half-width, $y_{\frac{1}{2}}$, is defined as the height from the wall where the velocity is half that of the maximum local velocity, as shown in figure 2.2. Similarly, as shown, the lateral half-width, $z_{\frac{1}{2}}$, is the distance across the jet at the height

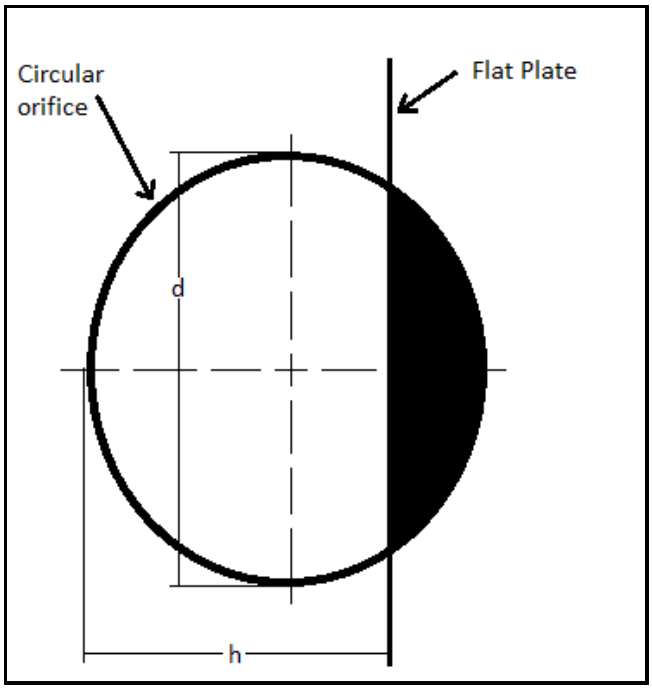

Figure 2.1: Orifice configuration employed by Padmanabham and Gowda .

of maximum velocity where the velocity is equal to half the maximum streamwise velocity.

Taking measurements of centerline velocity decay from the orifice jet described above, Viets and Sforza [7] observed that the development of the jet could be broken down into three regions: 1) The near-field, the area of the jet where the maximum velocity is the same as the exit velocity of the jet, also referred to as the potential core region, 2) The intermediate field, after the potential core has collapsed, but where the jet development is still sensitive to the particular geometry of the jet exit and lastly 3), the far-field or radial decay region where the flow approaches self similarity. Recently, Hall and Ewing [11] have questioned the existence of these three regions. Using the defined terms discussed previously (by Hall and Ewing), the region where the wall jet still resembles the outlet will be called the near-field, the far-field will be where the flow approaches similarity (in the mean), and the region in between these will be the intermediate field.

In general, several authors [16, 15, 10, 3, 17, 18] have concluded that $y_{\frac{1}{2}}$ and $z_{\frac{1}{2}}$

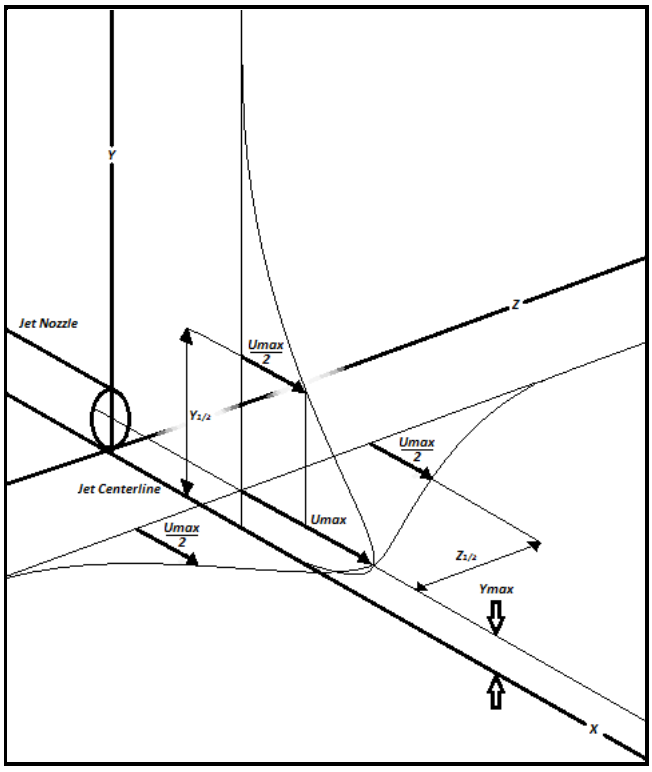

Figure 2.2: Three-dimensional wall jet schematic showing wall jet nomenclature.

grow linearly in the far-field. The growth rate of $y_{\frac{1}{2}}$ and $z_{\frac{1}{2}}$ in the far-field for various investigations are summarized in Table 2.1. In this table, h represents the distance from the top of the nozzle to the wall, as shown in figure 2.3. In order to account for the differences in the outlet size of the various jets. In Hall and Ewing [19] work it was proposed that the initial lateral and normal half-widths of the jet should be subtracted in order to relate the different geometries together on the same scale; this was particularly true for Hall and Ewing's large aspect-ratio jets. Looking at figure 2.4 and figure 2.5 Hall and Ewing showed that the data for the streamwise development of the lateral and normal half-widths from a number of investigations collapsing onto each other after those initial geometric differences are accounted for.

In general, it has been found that the mean streamwise velocity profiles become self-similar in the far-field when they were scaled using the local maximum streamwise velocity and the half-width of the jets. Compiling all the information available from

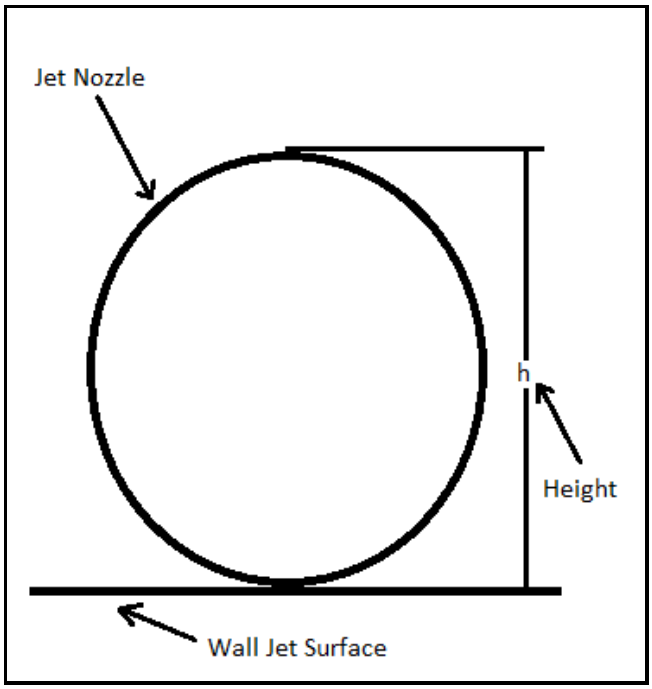

Figure 2.3: Three-dimensional wall jet highlighting the representation of h used in Table 2.1.

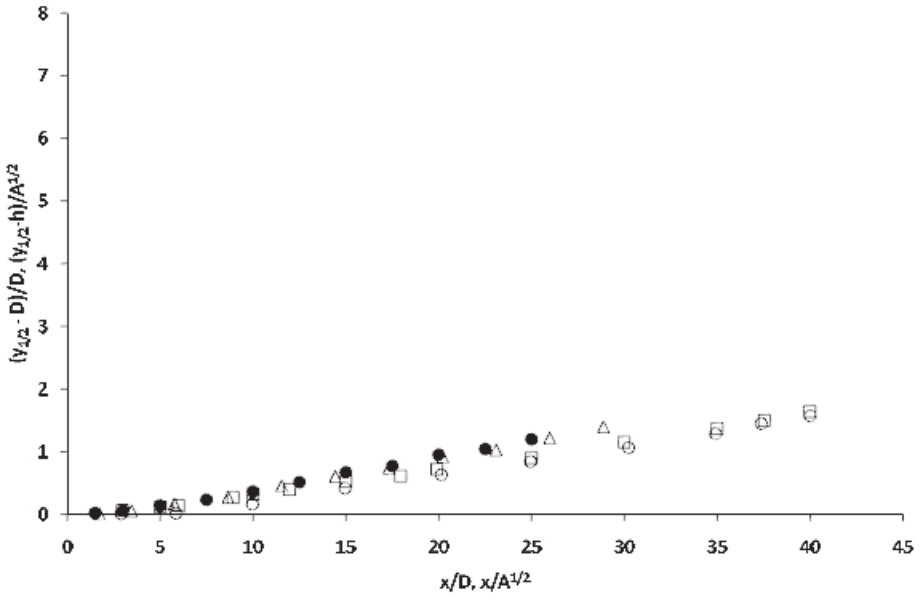

Figure 2.4: Normalized streamwise development of vertical half-widths for wall jet formed using a rectangular nozzle with $A_r = 1(\triangle)$ and $A_r = 4(\bullet)$ Hall [1], with a contoured nozzle ($\square$), and with long pipe ($\circ$) Sun [2].

Table 2.1: Summary of previous three-dimensional wall jet investigations.

Investigators	Nozzle Geometry	Region (x/D)	Re_{exit}	$\frac{\partial y_{1/2}}{\partial x}$	$\frac{\partial z_{1/2}}{\partial x}$	$\frac{\partial y_{1/2}/\partial x}{\partial z_{1/2}/\partial x}$
Abrahamsson *et al* [16]	Contoured Nozzle-Top Hat	50-90	79,000	0.065	0.32	4.92
Padmanabham and Gowda [15]	Segment		95,400			
	h/D=0.23	50-120		0.040	0.250	6.25
	h/D=0.50			0.049	0.245	5.00
	h/D=0.80	20-100		0.043	0.215	5.00
	h/D=1.00			0.045	0.216	4.80
Maslov *et al* [10]	Contoured Nozzle-Top Hat	50-350	100,000	0.056	0.30	5.34
		150-350		0.057	0.31	5.44
Davis and Winarto [3]	Contoured Nozzle-Top Hat		170,000			
	h/D=1.0	40-48		0.037	0.32	8.65
	h/D=1.50	40-56		0.036	0.33	9.17
	h/D=2.80	48-64		0.039	0.29	7.44
	h/D=4.5	48-56		0.046	0.23	5.00
Sun and Ewing [17]	Contoured Nozzle-Top Hat	35-40	108,000	0.053	0.27	5.09
Hall and Ewing [18]	Rectangular Nozzle-Fully Developed	3-40	89,600	0.051	0.28	5.5

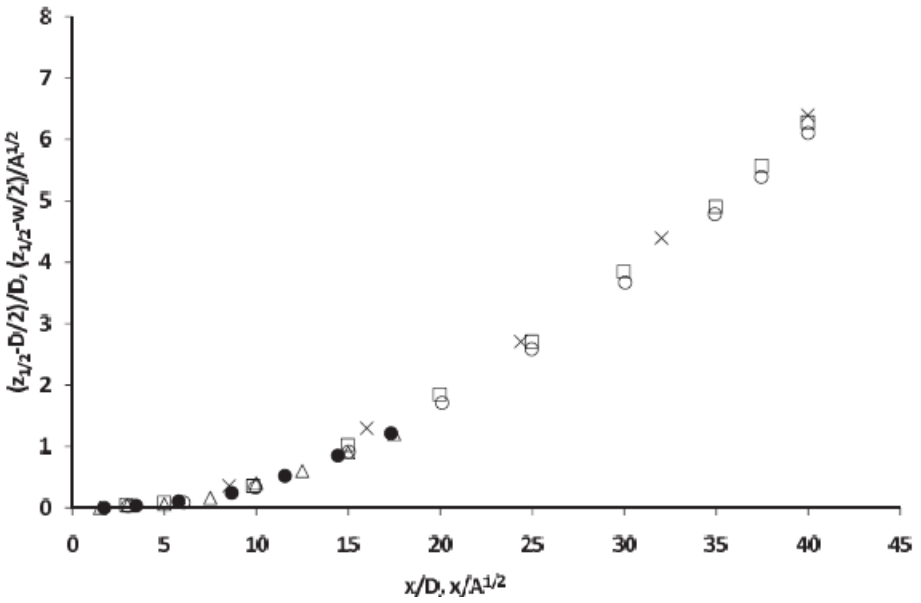

Figure 2.5: Normalized streamwise development of lateral half-widths from a jet exiting a rectangular nozzle with $A_r = 1(\triangle)$ and $A_r = 4(\bullet)$ Hall [1], with a contoured nozzle ($\square$) Sun [2], ($\times$) Davis and Winarto [3] and with long pipe ($\circ$) Sun [2].

early investigations in a review of studies, Launder and Rodi [9] concluded that the general growth rate normal to the wall was $0.048 + / - 0.002$ and the growth rate laterally was 0.26. This sets a lateral to vertical spreading ratio of 5.4:1. The compilation by Launder and Rodi excluded three-dimensional wall jets created with sharped-edged orifices; it was shown by Schwab [20] that jets created using sharp-edge orifices, such as Sforza and Herbst's[21], were facility specific and would always differ when compared to jets formed using other outlet conditions. Schwab's work revealed that a possible cause of this uniqueness to each orifice jet facility was the *vena contracta* developed inside the orifice at the jet exit, and the result being that it lead to a decrease in the lateral half-widths coming from the jet in the near-field.

2.2 Secondary Flow

Despite all the work completed on the three-dimensional wall jet, questions about the causes of the large anisotropy of the growth rates in the wall jet still puzzle

researchers. In Launder and Rodi's [9] review, it was proposed that the anisotropic growth of the jet had to be the result of mean secondary flows in the jet and that it would be best to understand this by examining the governing equations of the mean streamwise vorticity,

$$\underbrace{\frac{D\Omega_x}{Dt}}_{A} = \underbrace{\Omega_x \frac{\partial U}{\partial x}}_{B} + \underbrace{\Omega_y \frac{\partial U}{\partial y} + \Omega_z \frac{\partial U}{\partial z}}_{C} + \underbrace{\frac{\partial^2}{\partial y \partial z}(\overline{v^2} - \overline{w^2})}_{D} + \underbrace{(\frac{\partial^2}{\partial z^2} - \frac{\partial^2}{\partial y^2})\overline{vw}}_{E} + \underbrace{\nu(\frac{\partial^2 \Omega_x}{\partial x^2} + \frac{\partial^2 \Omega_x}{\partial y^2} + \frac{\partial^2 \Omega_x}{\partial z^2})}_{F} \quad (2.1)$$

where

$$\Omega_x = \frac{\partial W}{\partial y} - \frac{\partial V}{\partial z} \quad (2.2)$$

$$\Omega_y = \frac{\partial U}{\partial z} - \frac{\partial W}{\partial x} \quad (2.3)$$

$$\Omega_z = \frac{\partial V}{\partial x} - \frac{\partial U}{\partial y} \quad (2.4)$$

Each of these terms can be summarized as follows:

A Transport of streamwise vorticity

B Streamwise amplification of mean vorticity by vortex stretching

C Vorticity production by vortex-line bending

D Vorticity production by gradient in Reynolds stresses

E Vorticity production by gradient in Reynolds shear stresses

F Viscous diffusion of vorticity

Looking at the terms in Equation 2.1, one possible source of streamwise vorticity in the wall jet could come from the vortex-line bending or tilting production term (term C). Breaking that term down gives,

$$\Omega_x \frac{\partial U}{\partial y} + \Omega_z \frac{\partial U}{\partial z} = \frac{\partial V}{\partial x}\frac{\partial U}{\partial z} - \frac{\partial W}{\partial x}\frac{\partial U}{\partial y} \tag{2.5}$$

Launder and Rodi [9] argued that due to scaling, the second term in Equation 2.5 would be dominant in the far-field of the three-dimensional wall jet. They proposed that there must be pairs of counter rotating mean streamwise vorticity on each side of the jet centerline in the $y-z$ plane as shown in figure 2.6. The explanation is that these regions of counter rotating vorticity push the fluid into the wall and laterally away from the centerline of the jet creating the large anisotropic growth pattern that is characteristic of the three-dimensional wall jet.

Craft and Launder[22] later argued that the vortex-tilting mechanism would also occur in the laminar jet, and that vortex tilting alone could not explain the large lateral growth. They argued that terms D and E must be responsible for the disparity. Namgyal and Hall [23] and Namgyal [24] have recently investigated this in detail, and found that the difference in the normal stresses caused by the wall was the largest contributor to the turbulent generated secondary flow.

Although the secondary flow in three-dimensional wall jets has not been well documented in the literature, the secondary flow in square ducts has received significant attention. Previously, secondary flows have been examined in square duct flow using both experimental and and numerical methods, these will be examined here because they are derived from similar source terms to the wall jet.

Prandtl's early work[25] proposed that there were two types of secondary flow, skew-induced (Prandtl's first kind) and stress-induced (Prandtl's second kind). The terms B and C from equation 2.1 are behind the creation of the first type mentioned.

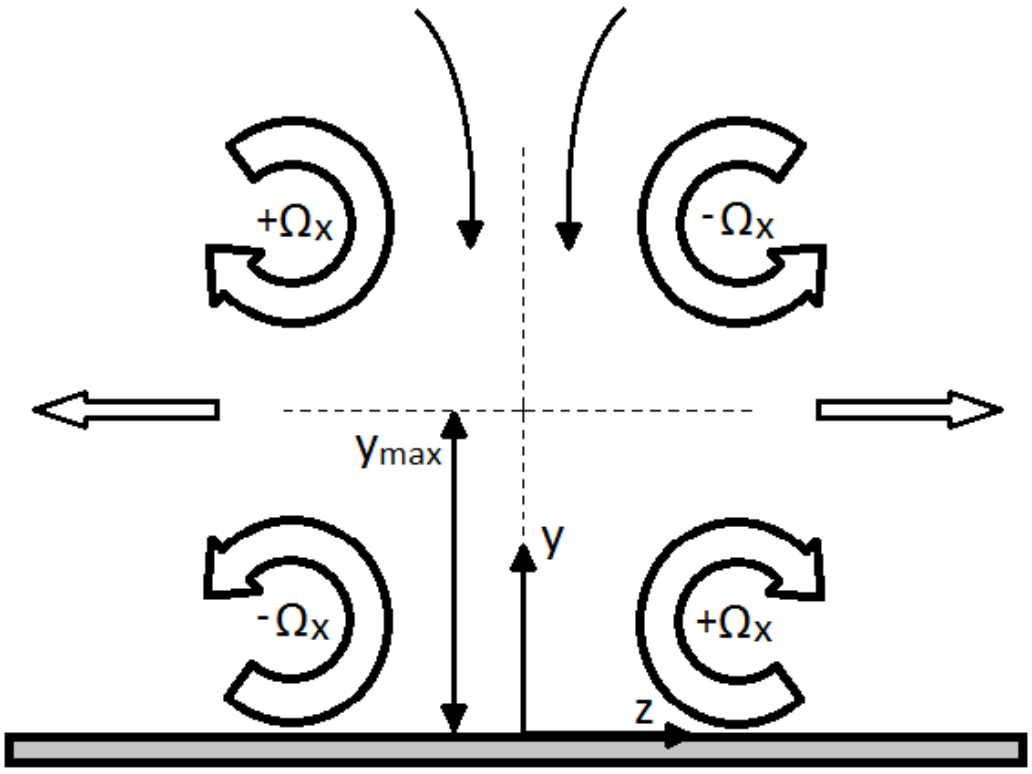

Figure 2.6: Streamwise vorticity model proposed by Launder and Rodi.

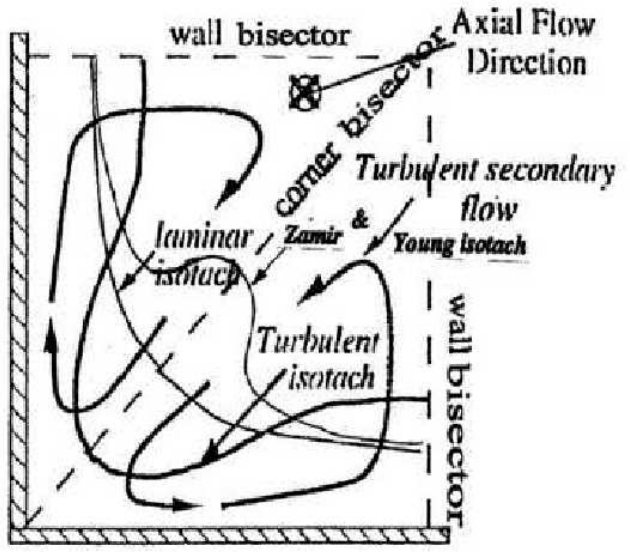

Figure 2.7: A sketch of flow structure in the internal corner region of straight duct (Gessner and Jones [4].)

The second kind is attributed to term D and term E. Prandtl recognized that turbulent flow in square ducts belong to the later kind of secondary flow mentioned above.

In square duct flow, the secondary flow velocities produced by turbulence are smaller then those in a three-dimensional wall jet. Studies like Gessner and Jones [4] show that the secondary flow along the along the corner bisector is directed inwards towards the corner in turbulent flow, the opposite of this occurs in similar laminar flow investigations of Zamir and Young [26]; a schematic of these processes are shown in figure 2.7. Measurement of the Reynolds stresses in a square duct, shown in figures 2.8, 2.9 and 2.10, were used by Brundrett and Baines [5] to argue that the addition of anisotropy from in plane shear stresses is minimal as the correlation shows that the magnitude is small in comparison to the normal stresses shown in figure 2.8 and 2.9; Namgyal [24] found the same in the turbulent three-dimensional wall jet. Brundrett and Bains also noted that the region of maximum production occurs just away from the wall as illustrated in figure 2.10.

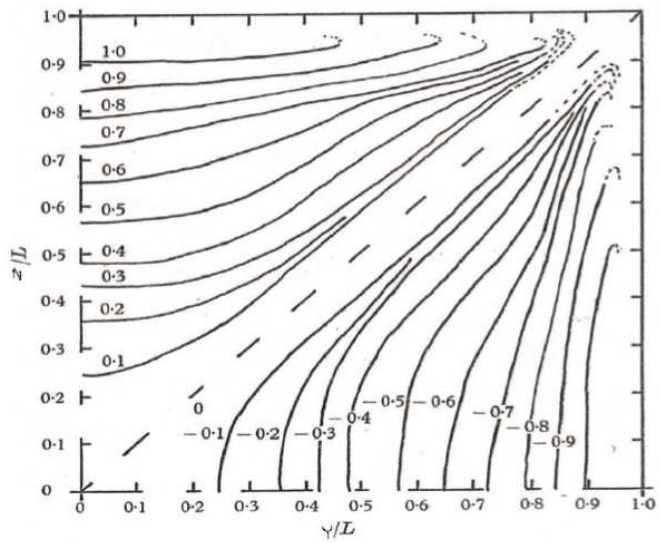

Figure 2.8: Reynolds stresses measured in a square duct flow (Wall is along top and right side), from Brundrett and Baines [5].

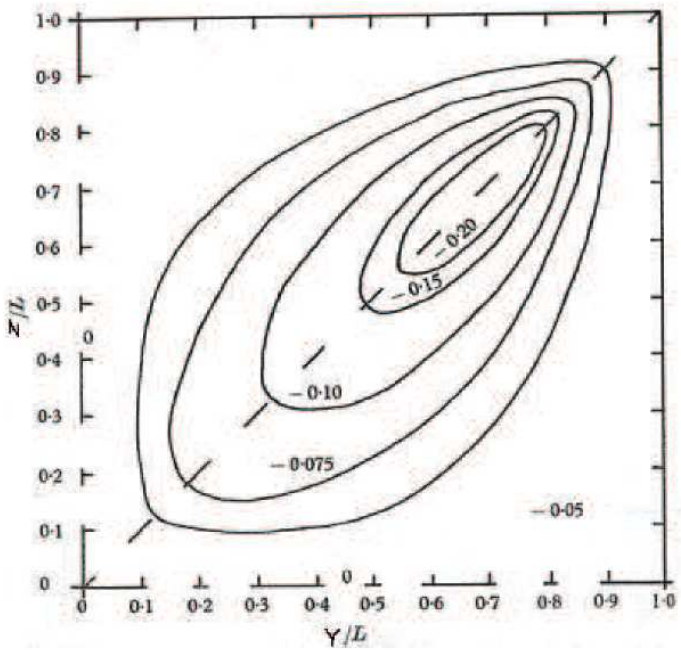

Figure 2.9: Reynolds stresses measured in a square duct flow (Wall is along top and right side), from Brundrett and Baines [5].

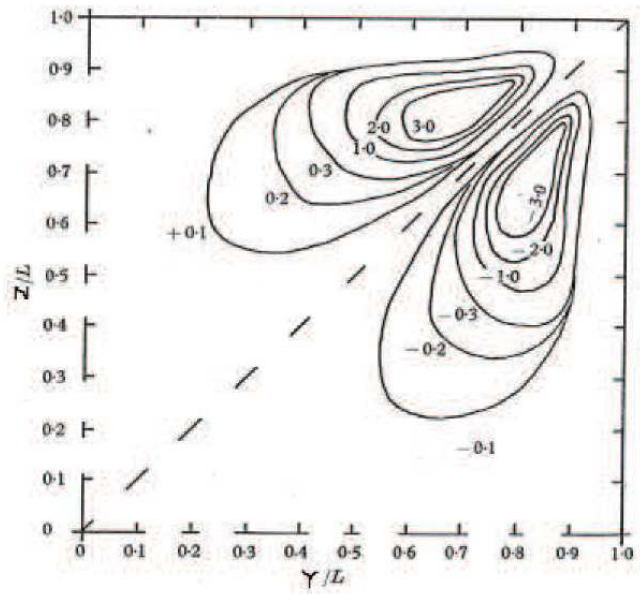

Figure 2.10: Reynolds stresses measured in a square duct flow (Wall is along top and right side), from Brundrett and Baines [5].

Numerical simulations have also been used to study flows in a straight annular square duct, for example Xu [27] performed a DNS on a fully developed turbulent flow in a square annular duct. The data showed that there was strong turbulent generated secondary flow along the corner bisector, this caused a moderate disturbance in the streamwise velocity contours at the corners. The disturbance in the corner alters the boundary layer in that region changing the flow so that it is different from that of the three-dimensional wall jet.

Hogg and Launder [6] have presented the only previous measurements in a corner wall jet; a diagram of the terms used in the jet apparatus is shown in figure 2.12. Hogg and Launder's jet was formed using a square duct. Hogg and Launder focused on downstream distances of $\frac{x}{D} = 40$ to 80 diameters. Mean velocity profiles measured normal to the wall taken by Hogg and Launder are shown in figure 2.11, they were collected along the corner bisector and show that there is a self-similar form when scaled by the half width and the local maximum velocity. They noted the jet achieved self-similar behavior in the mean at $\frac{x}{D} = 40$ which is relatively consistent with

observations in the three-dimensional wall jet.

Hogg and Launder also did a complete mapping of the mean velocity at 50 diameters downstream, as shown in figure 2.13. Here the flow spreads out along the walls and it can be seen that the bisector is indeed the point of symmetry. Hogg and Launder argued that, like the three-dimensional wall jet, the fluid is drawn into the corner along the bisector and pushed out along the walls by secondary flow moving parallel to the walls. They also argued that this behavior is not as strong in the corner wall jet as the flat wall jet as the angle of spread is half as large (as shown in figure 2.14). Hogg and Launder found that the growth of the bisector half-width is also approximately a third larger in the corner wall jet then the vertical half-width of the flat wall jet. Hogg and Launder suggests that these differences can be attributed to increased wall friction. It should be noted that Hogg and Launder performed their measurements with a pitot tube, and thus no measurements of the unsteady turbulent velocity could be performed.

The current work aims to expand upon the measurements by Hogg and Launder by examining the early development of the jet, from the near-field and on to the far-field, from $\frac{x}{D} = 0$ to 40. The present study will measure both the mean and turbulent streamwise velocities using hot-wire anemometry. The three-dimensional wall jet will be formed using the flow from a fully developed pipe flow. This differs from Hogg and Launder who used a fully developed square duct flow. As discussed, a square duct flow already possess secondary flow, so a round pipe was selected as it has no pre-existing secondary flow.

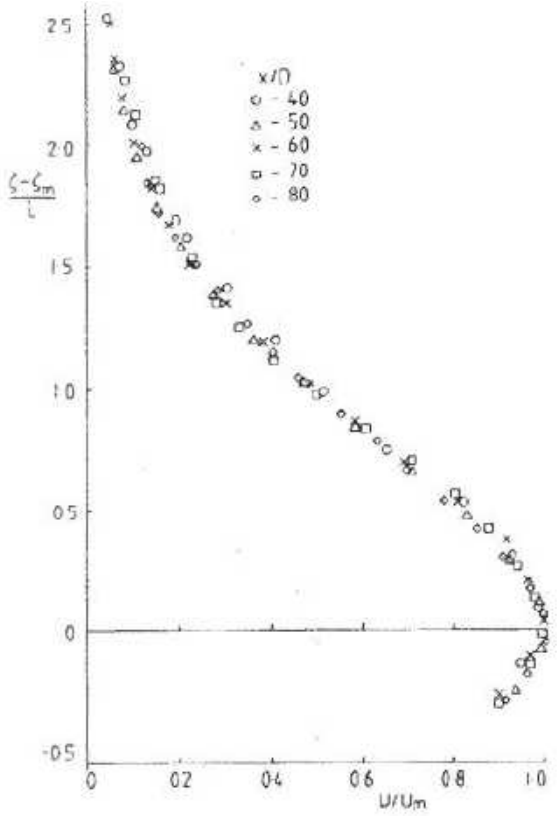

Figure 2.11: Mean velocity profiles in a corner wall jet by Hogg and Launder [6].

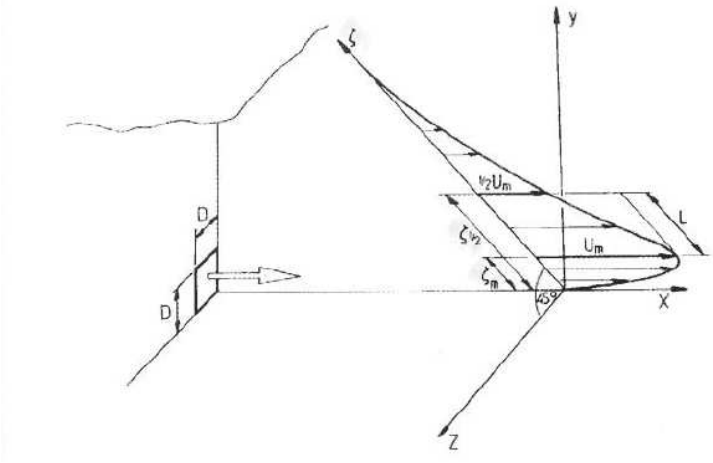

Figure 2.12: Diagram of terms used in a corner wall jet by Hogg and Launder [6].

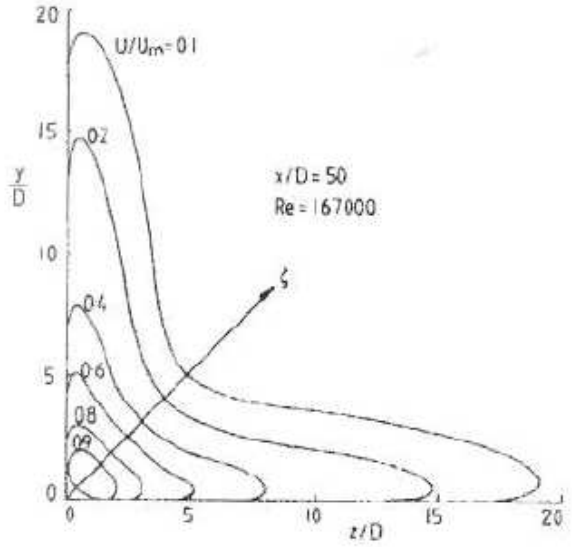

Figure 2.13: Velocity contours measured in the corner wall jet at 50 diameters downstream by Hogg and Launder [6].

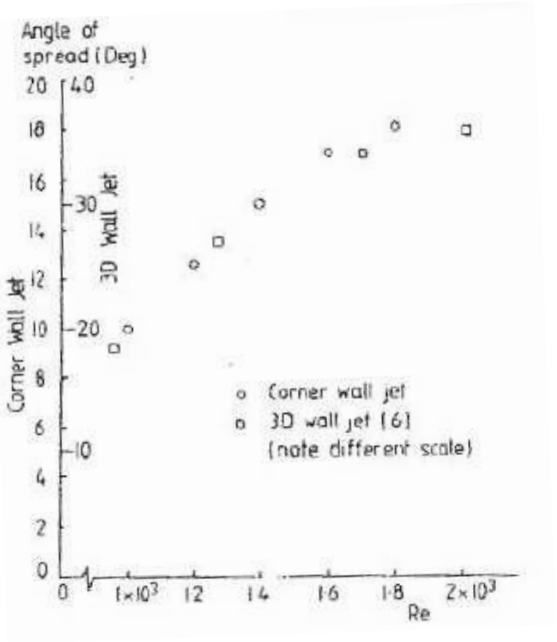

Figure 2.14: Angle of spread measured in far-field of corner wall jet by Hogg and Launder [6].

Chapter 3

Experimental Setup

The following chapter discusses the experimental facility developed at UNB to study the corner wall jet. An schematic of the experimental facility is shown in figure 3.1.

The frame of the wall jet facility is constructed of $38mm$ by $38mm$ square steel tubing held together with both bolts and welds. The frame is the shape of a rectangle approximately $1.87m$ tall, $1.22m$ wide and $1.27m$ long. Inside the outer frame, which is mostly welded, is a removable shelf that bolts to the frame, this shelf is used to secure and manipulate the surface that the jet flows over and can also be removed completely to create space for a free jet. The shelf is $1.17m$ tall and $1.22m$ wide.

Attached to the top of the frame along the width is the three-dimensional traverse used to move the probe around the test space, it consists of two width spanning parallel solid core chrome plated cylinders one inch in diameter and $0.65m$ apart. Four one inch bushings attach to the aluminum frame to facilitate movement along the streamwise axis (X). The aluminum frame holds smaller but similar traversing mechanisms for lateral and vertical movement (Z and Y). Each axis of the traverse is measured by a divisional tape measure and a pointer that moves with the particular axis along the tape.

Resting on the internal shelf is a $0.58m$ by $1.41m$ sheet of Medium Density

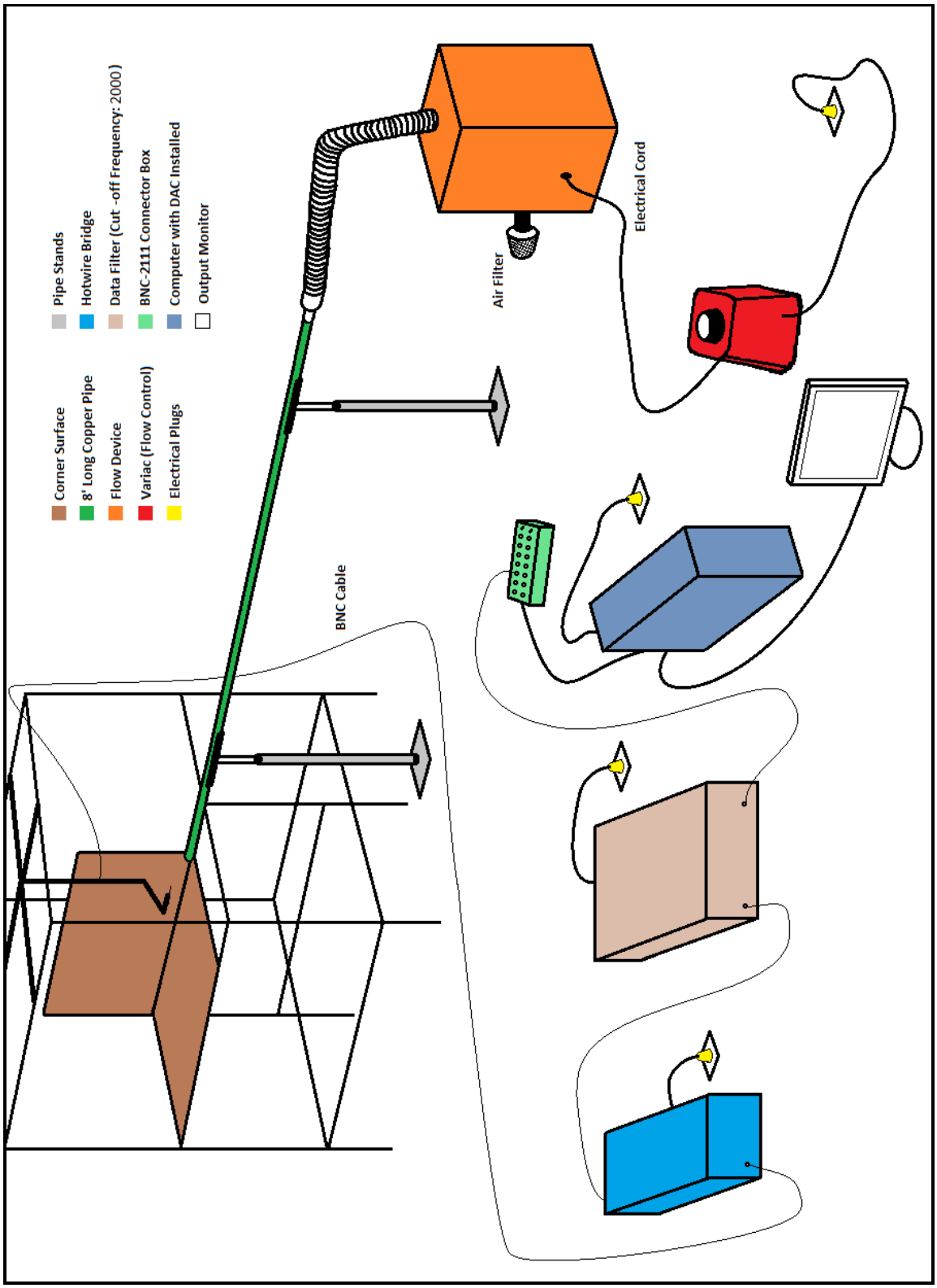

Figure 3.1: Schematic of corner wall jet facility.

Fiberboard (MDF), it serves as the surface for the jet flow to move over as it is quite smooth. Adjacent to the horizontal MDF sheet is a larger sheet of MDF positioned vertically and parallel to the centerline, this creates a 90° corner between the two pieces of MDF when both pieces are properly adjusted using a laser level and metal shims. The piece of MDF that forms the vertical wall is held in place by a second metal shelf that rests inside the external frame, this is just enough space for the MDF to sit vertically with a little room to place wedges along the back side of the sheet to push it up against the horizontal MDF sheet, which is braced against the other side of the external frame, creating a tight seal for the corner that does not allow for the leakage of fluid but also does not deform the sharp smooth corner.

Extending parallel along the vertex of the corner approximately $200mm$ from the edge is a $25.4mm$ diameter copper pipe that is $2.56m$ long and is placed such that the centerline is as close to the vertex as possible as shown in figure 3.2, this means that the pipe wall intersects tangentially along the surface of both the vertical and horizontal MDF surfaces. The pipe is aligned and leveled using the back wall behind the pipe and a laser level, this is done to ensure that the jet issuing from the nozzle does so without deflection into or away from the wall surface which would alter the evolution of the jet profiles. The pipe rests on two steel stands with substantial plates for base support and angle iron to rest the pipe along. The height of pipe can be adjusted by the nuts and bolts in place at both the plate and beneath the angle iron, this helps with leveling and aligning the pipe.

At the end of the copper pipe is an adapter that connects the pipe to a hose used to transport the flow from the blower to the pipe, the adapter is sealed to prevent fluid from leaking out or particles from getting into the jet. The blower uses a universal motor to pump air from inside of a sealed chamber that collects air through a filtered pipe attachment fitted to the blower, it extends off the base and has a foam insert that keeps the intake air clear of large particles. The blower

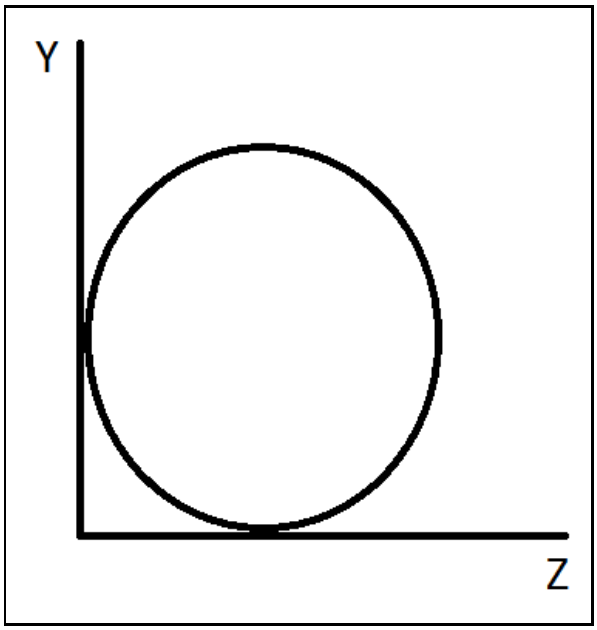

Figure 3.2: Pipe positioning for corner wall jet.

was manufactured by Ridgid, model number WD1851. The speed of the blower was varied using a variac or variable autotransformer.

Magnetically attached to the side of the outer frame is a simple u-tube manometer from Dynson. This is used in conjunction with a Pitot-static tube to get the velocity of the jet exit when doing calibration of the hot-wire. The pressure in inches of water is read off the manometer and then converted to velocity.

The turbulent velocity was measured using a hot-wire probe; a $5\mu m$ tungsten Dantec hotwire probe was ran with an overheat ratio of 1.8. The hot-wire probe sits inside the probe seat which then has a single wire that runs out the back and is connected to a $5m$ long BNC cable. The probe seat is made of aluminum and has a top that screws on to secure the wire in place.

Holding the probe seat is a custom built probe holder, the probe seat slides inside the probe holder at the desired angle, preferably 0° or 90° depending on what direction the probe is moving wile taking data, and is held in place by a set screw. The probe holder was constructed from a stainless steel tube with $\frac{1}{4}inch$ diameter and and $\frac{1}{16}inch$ thickness with a 90° gentle bend at the bottom. The backside of the

gentle bend has been removed to allow enough room for the wires coming from the probe seat to slide up inside the probe holder tube and out the top.

The wire that comes off the probe holder goes into a series of BNC adaptor connections and is then wrapped in electrical tape to prevent interference from other sources touching the connection wile the setup is active and burning out the wire.

The $5m$ long BNC connector makes it's way back around the frame and into the front of the hot-wire bridge. The bridge the probe connects to is a DISA CTA BRIDGE 56C17 with a DISA type 56C01 CTA card. It is balanced and has a bridge adjustment of 38Ω's. The output from the bridge leaves via BNC connection port one and travels over to the filter unit.

The filter is a Krohn-Hite Corporation produced Model 3364 Filter 4 pole LP/HP Butterworth/Bessel. The signal leaving the bridge enters on CH 1+ and is set to be low-pass filtered at a cutoff frequency of $2000Hz$ on the DC setting with no gain(dB) on either input or output, the type of filter is set to Butterworth. The signal leaves the filter via CH1 and is sent to the BNC connector box.

The BNC connector box is a National Instruments BNC-2111 and serves as the interface between the data acquisition card or DAQ and the signal coming in from the hot-wire. The BNC was connected on analog input nine (AI9) and the switch set to NRSE.

The hot-wire outputs voltage and requires calibration to convert it to velocity data. In order to do this several numbers were chosen between the maximum and minimum range of inches of water, on the manometer, that the jet could push and the jet speed was varied up or down using the variac dial until the desired number of inches of water was reached. The hot-wire was then traversed into place and and a measurement was taken in the center of the jet. After several points were taken in this manner a table of jet velocity verses hot-wire voltage was created in excel and a fourth-order polynomial was curve fit to it thus giving a calibration curve and

equation that could be used to change all the voltage data for a particular run into velocity data.

The DAQ takes the voltage signal it receives from the hot-wire and converts them into digital values that can then be manipulated by the computer. The DAQ card is installed into the computer along with driver software. This particular DAQ is a NI PCI 6229 card and can sample up to 260000 samples per second. Here, the data was sampled at a block length of 4096 samples every second for however many blocks of data are desired. In the case of the free jet and the three-dimensional wall jet 300 blocks of data were taken per point which is about five minutes; in the case of the corner wall jet 60 blocks of data were taken per point or one minute. The data is then stored in a specified directory structure that records it's position on the X, Y and Z axis and the date of the test as well as what type of traverse was completed be it either vertical or horizontal. The program does do some basic data analysis to check and see if the information coming in is reasonable or the test needs to be repeated. It includes a table that contains the time and voltage acquired for that particular run as well as a mean value for the voltages in that table and a power spectra analysis on a block by block basis or on all blocks combined.

3.1 The Free Jet

Mean and turbulent velocity profiles were taken at the pipe exit of $0.01D$. The velocity axis was normalized by the jet exit velocity which in this case is $50m/s$. The traversing axis was normalized by the diameter of the jet represented by D. As shown, the mean flow at the jet exit is symmetrical flow about the vertical axis (figure 3.3) and in good agreement with the generally accepted 1/7th power profile for fully developed pipe flow. A similar profile measured across the jet in the horizontal direction (figure 3.4) is also symmetrical and in good agreement with the accepted

profile for fully developed pipe flow. Together, these results demonstrate the the jet is developing properly and indicates that the flow exiting the pipe is fully developed.

Profiles of the turbulent intensity are also shown in figure 3.3 and figure 3.4. In this case, the profiles are again symmetrical about the axis within the jet diameter as well as being very similar to each other in shape and size. The turbulent velocity increases fairly linearly across the jet outlet consistent with measurements in a pipe jet by Sun [2] and Hall [1].

Power spectra at the jet outlet was also computed to ensure that the jet was behaving properly. Figure 3.5 shows the power spectrum taken at the center of the jet outlet. In general, the spectrum is reasonably broadband, and does not exhibit many narrow band peaks that could be indicative of noise: one exception, though, is the peak at $120Hz$. This was experimentally determined to be the blade pass frequency of the blower. There is another very small peak in the 30 diameter downstream position at $10,000Hz$, this peak is very sharp and is believed to be electrical background noise from the blower motor.

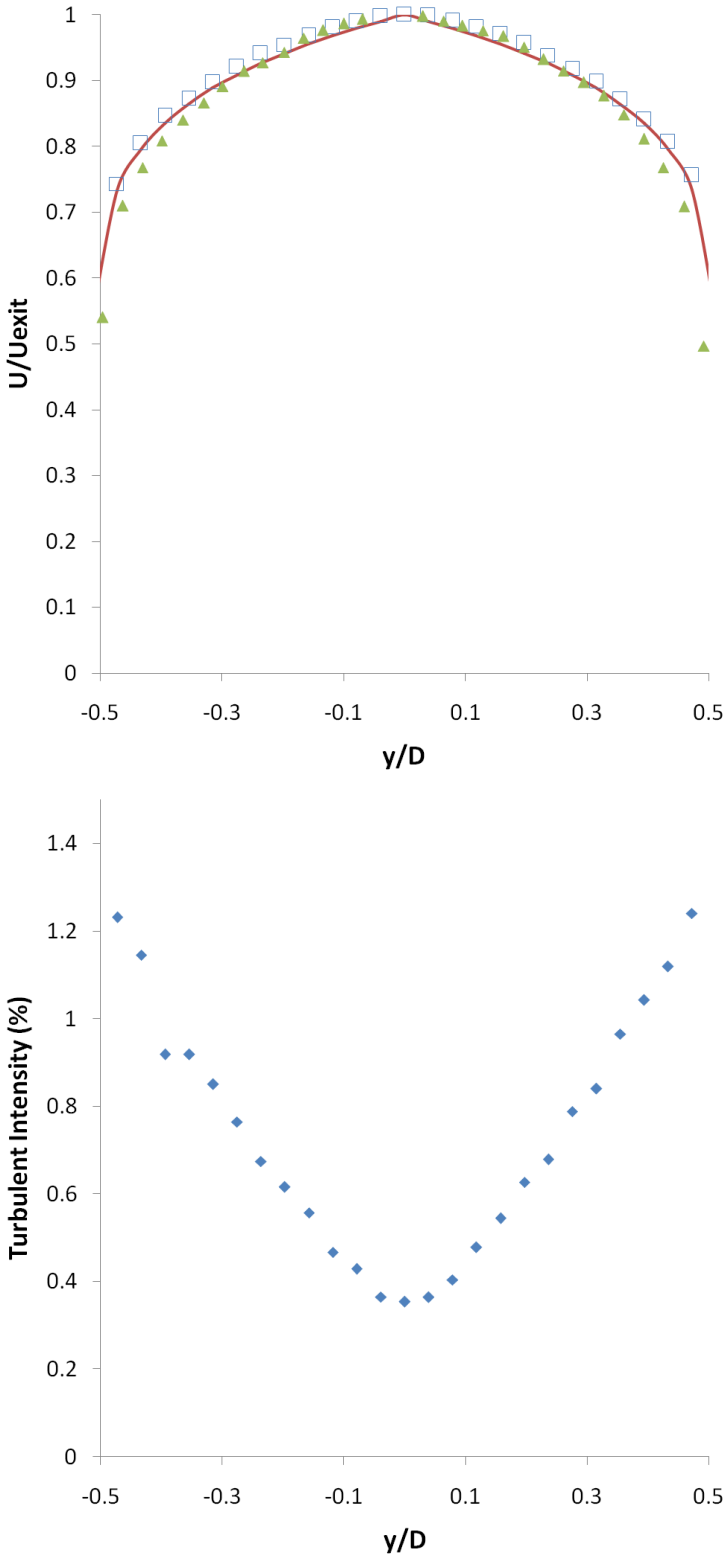

Figure 3.3: Vertical profile (top) of mean velocity and turbulent intensity (bottom) of a free jet taken at the exit. Mean Velocity (□), Ideal 1/7th power law profile(-), Mean Streamwise Velocity(▲) from Sun [2] and Turbulent Intensity(⧫).

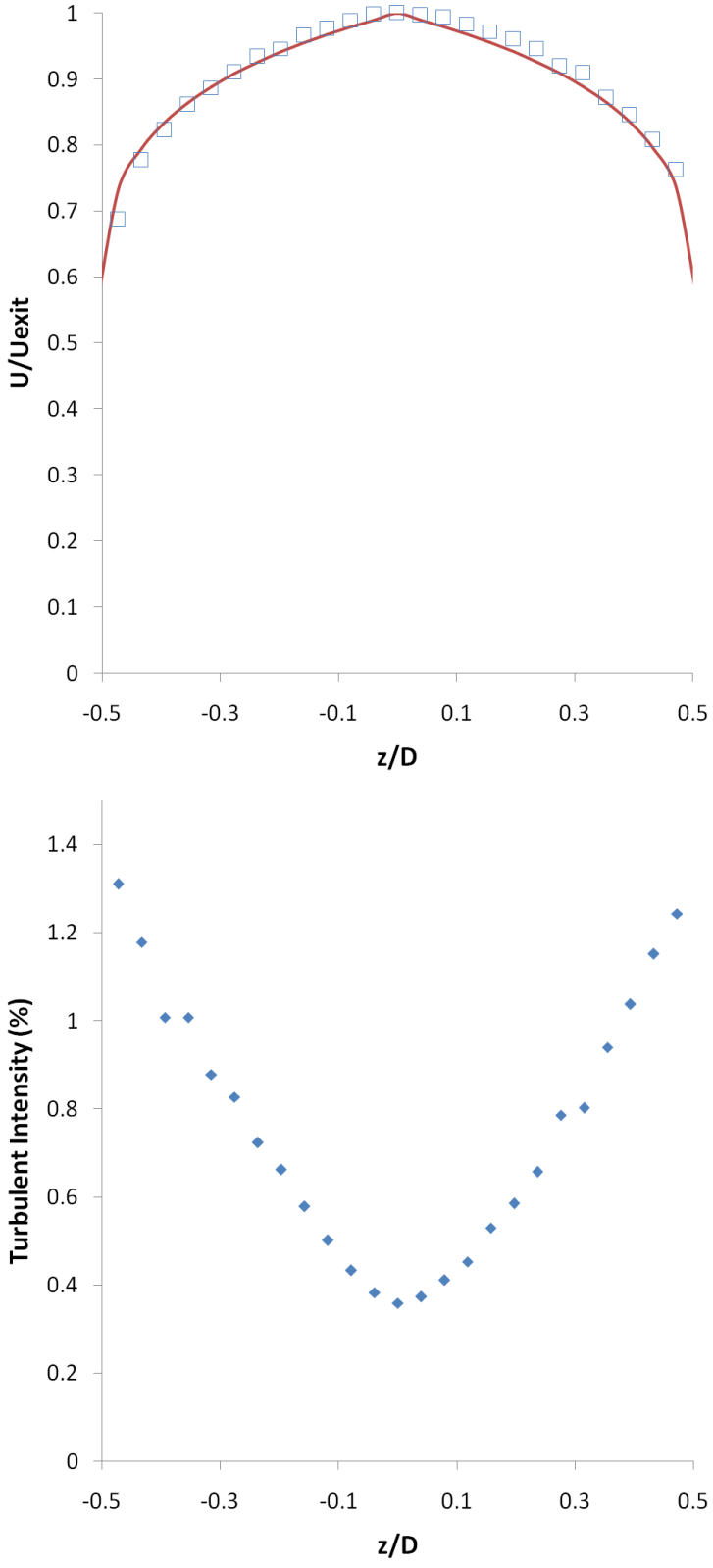

Figure 3.4: Horizontal profile (top) of mean velocity and turbulent intensity (bottom) of a free jet taken at the exit. Mean Velocity (□), Ideal 1/7th power law Profile(-), Mean Streamwise Velocity(▲) from Sun [2] and Turbulent Intensity(♦).

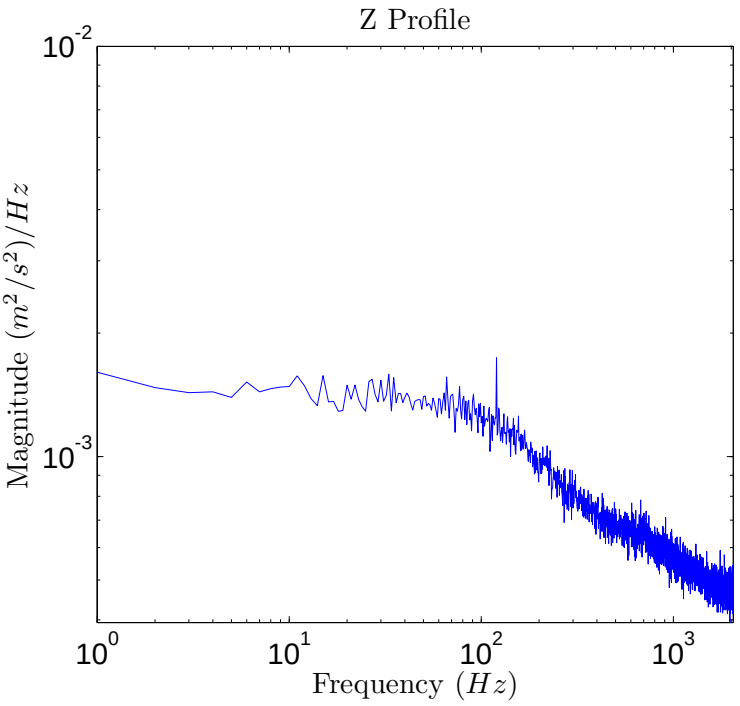

Figure 3.5: Power Spectrum measured at the center of the jet outlet center from the z profile or horizontal.

Chapter 4

Experimental Results and Discussion

4.1 The Three-Dimensional Wall Jet

Mean and turbulent velocity profiles measured in the near-field and on the jet centerline are shown in figure 4.1. Here, the profiles have been normalized using U_{max} and D. The profile taken at $\frac{x}{D} = 0$ strongly resembles the velocity profile for turbulent pipe flow, as expected. Downstream, the profiles at the 2 and 5 diameter positions show that the jet develops in towards the wall slightly and begins to lose the characteristics of the turbulent pipe flow profile. This has been noted by several researchers [3, 1, 9, 2] and is caused by the rapid lateral development of the jet. As the flow evolves further downstream it is affected more by the wall surface and by $\frac{x}{D} = 10$ the point of maximum velocity, U_{max}, moves outward away from the wall.

The turbulent intensity profile in figure 4.1 shows that the turbulent intensity is initially very low in the middle and high near the walls, as expected for fully developed pipe flow. As the jet evolves downstream, the turbulence intensity increases and the peak associated with the outer shear-layer grows faster than the

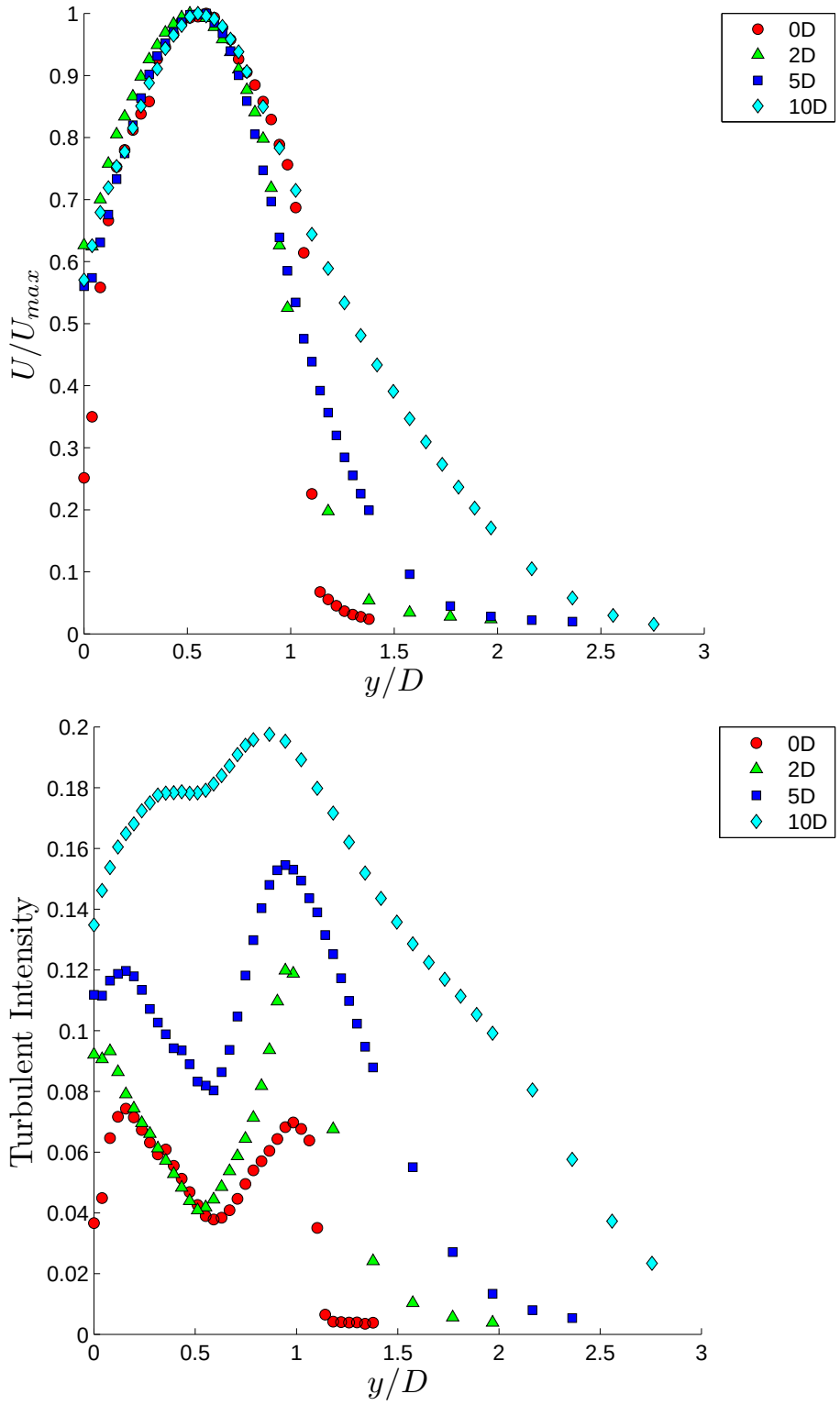

Figure 4.1: Profiles of the mean velocity (top) and turbulent velocity (bottom) measured on the jet centreline of a three-dimensional wall jet in the near-field.

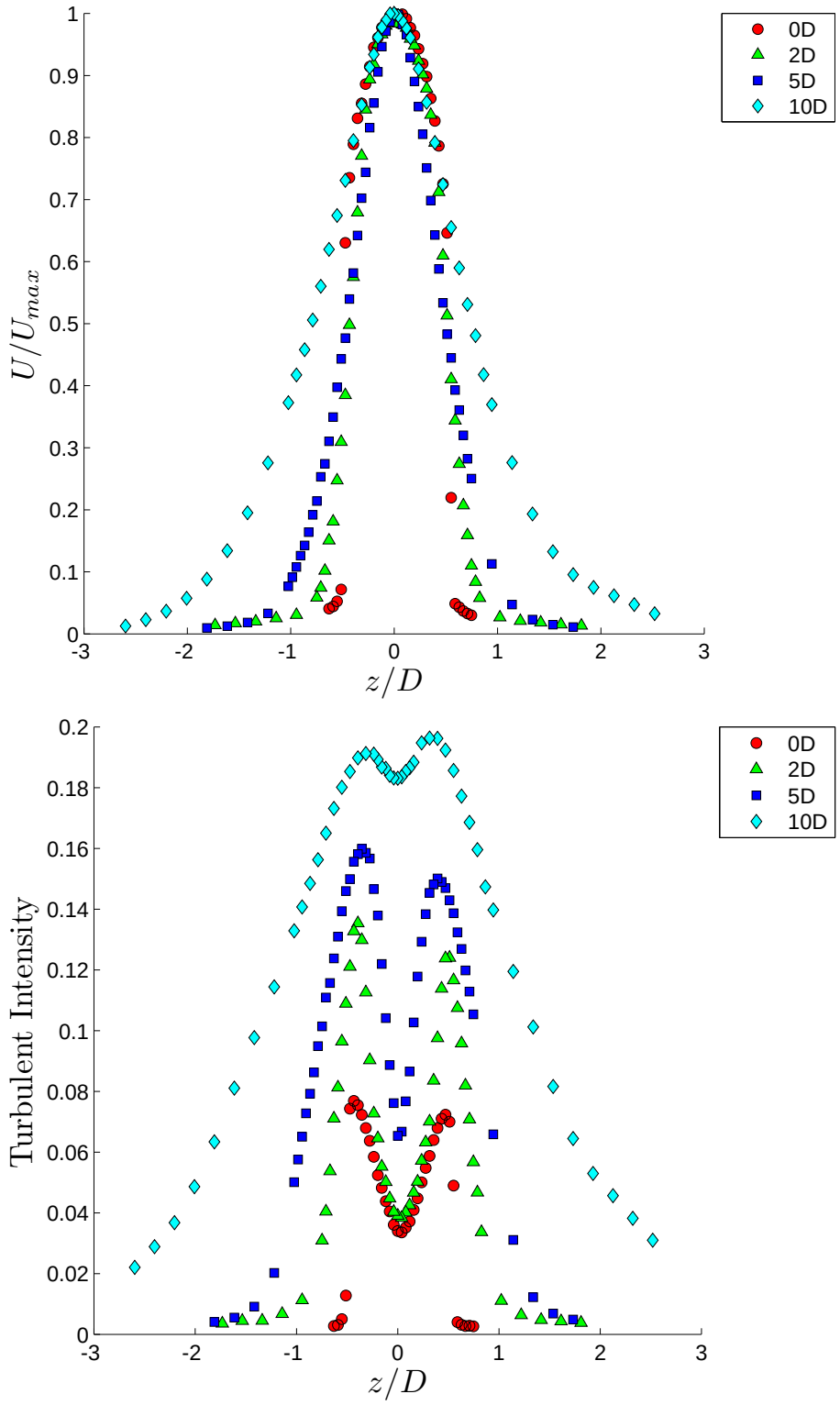

Figure 4.2: Profiles of the mean velocity (top) and turbulent velocity (bottom) measured across the jet at y_{max} in the near-field of a three-dimensional wall jet.

inner peak. At approximately 10 diameters downstream the pronounced minima has almost disappeared and the turbulent intensity associated with the outer peak becomes dominant. Again, this behavior is consistent with previous studies in the three-dimensional wall jet (i.e Sun[2], Hall[1]).

Mean and turbulent velocity profiles were also measured in the near-field of the wall jet, but this time across the jet at the height of the maximum velocity point. These profiles are shown for the $\frac{x}{D} = 0$, 2, 5 and 10 positions in figure 4.2. Initially, the mean velocity profile looks much like a turbulent pipe flow profile. As the flow evolves downstream, the mean profile widens slowly from $\frac{x}{D} = 5$ to 10, then the jet begins to grow rapidly in the lateral direction. In all cases the profiles of turbulence intensity have two peaks associated with the lateral shear-layers on either side of the jet centerline. The magnitude of the peaks grow and widen as the jet evolves downstream and eventually begins to merge at $\frac{x}{D} = 10$.

Similar profiles of the mean and turbulent streamwise velocity in the intermediate to far-field are shown in figure 4.3 and figure 4.4. The profiles from $\frac{x}{D} = 10$ shown in the previous figure are included for comparison. In this case the profiles are normalized by U_{max} and D. In the mean profiles measured normal to the wall, on the jet centreline, the outward growth of the jet is clearly observed. The profiles of turbulence intensity initially show two peaks at $\frac{x}{D} = 10$, but as the jet evolves downstream the outer peak associated with the outer shear-layer grow in intensity, gets broader and moves away from the wall. The mean profiles measured across the jet get significantly wider showing the rapid lateral development of the three-dimensional wall jet. This rapid growth is accompanied by a spreading of the two peaks in the turbulence intensity. As the jet develops downstream these peaks spread apart and become broader.

Profiles of the mean and turbulent streamwise velocity in the intermediate to far-field are again shown in figure 4.5, however, in this case, again the velocities are

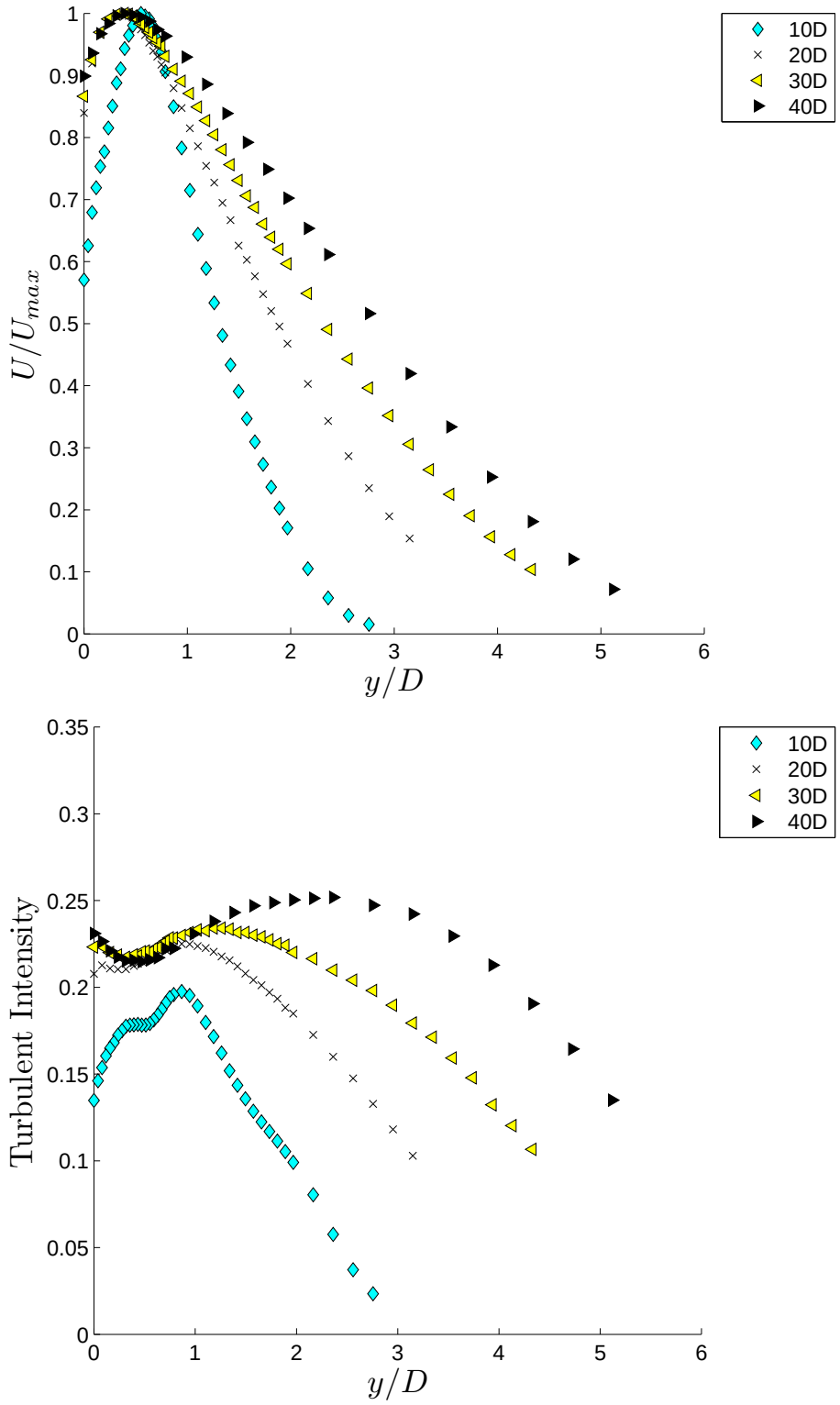

Figure 4.3: Profiles of the mean (top) and turbulent velocity (bottom) measured on the jet centreline in the intermediate to far-field region.

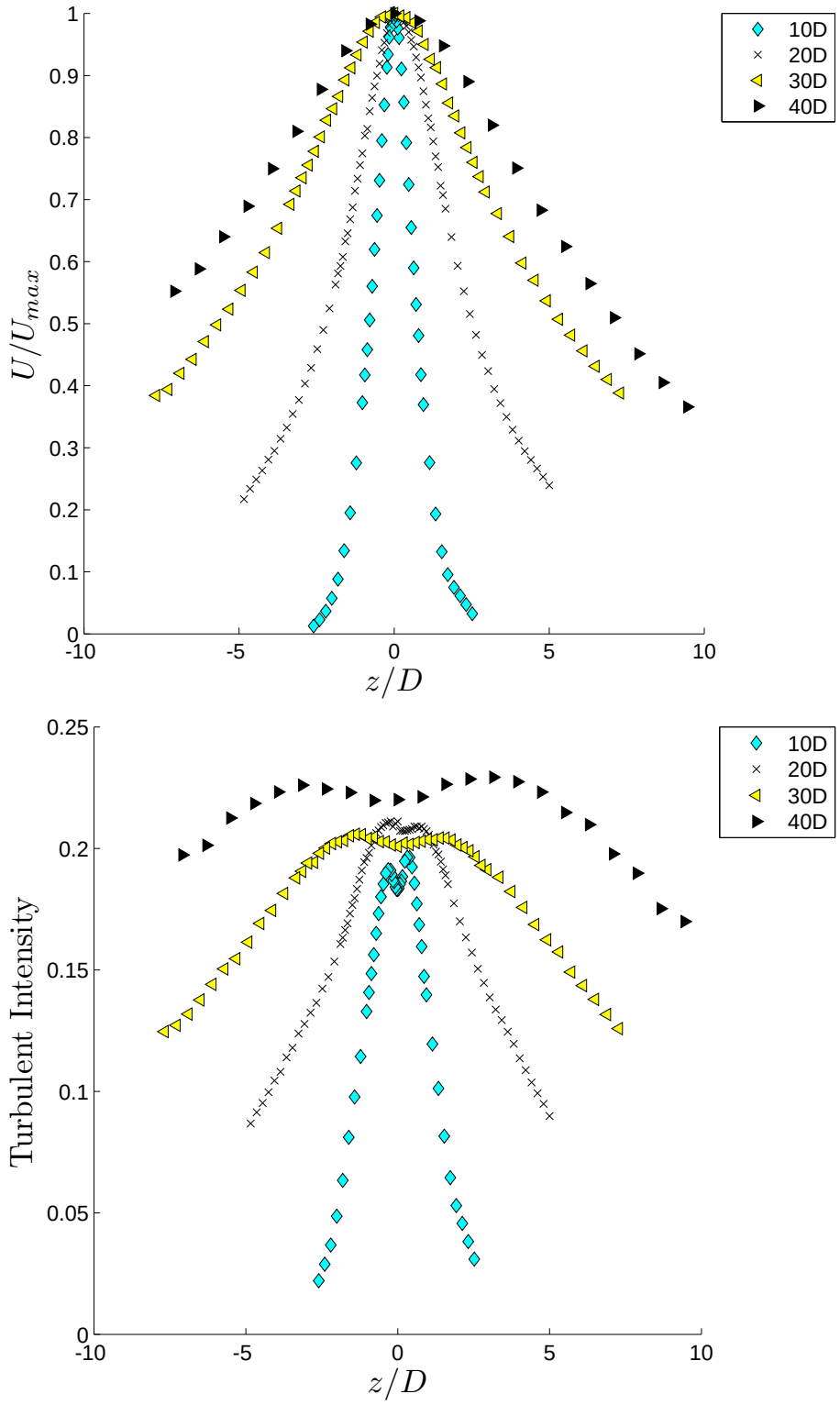

Figure 4.4: Profiles of the mean (top) and turbulent velocity (bottom) measured across the jet at y_{max} in the intermediate to far-field region.

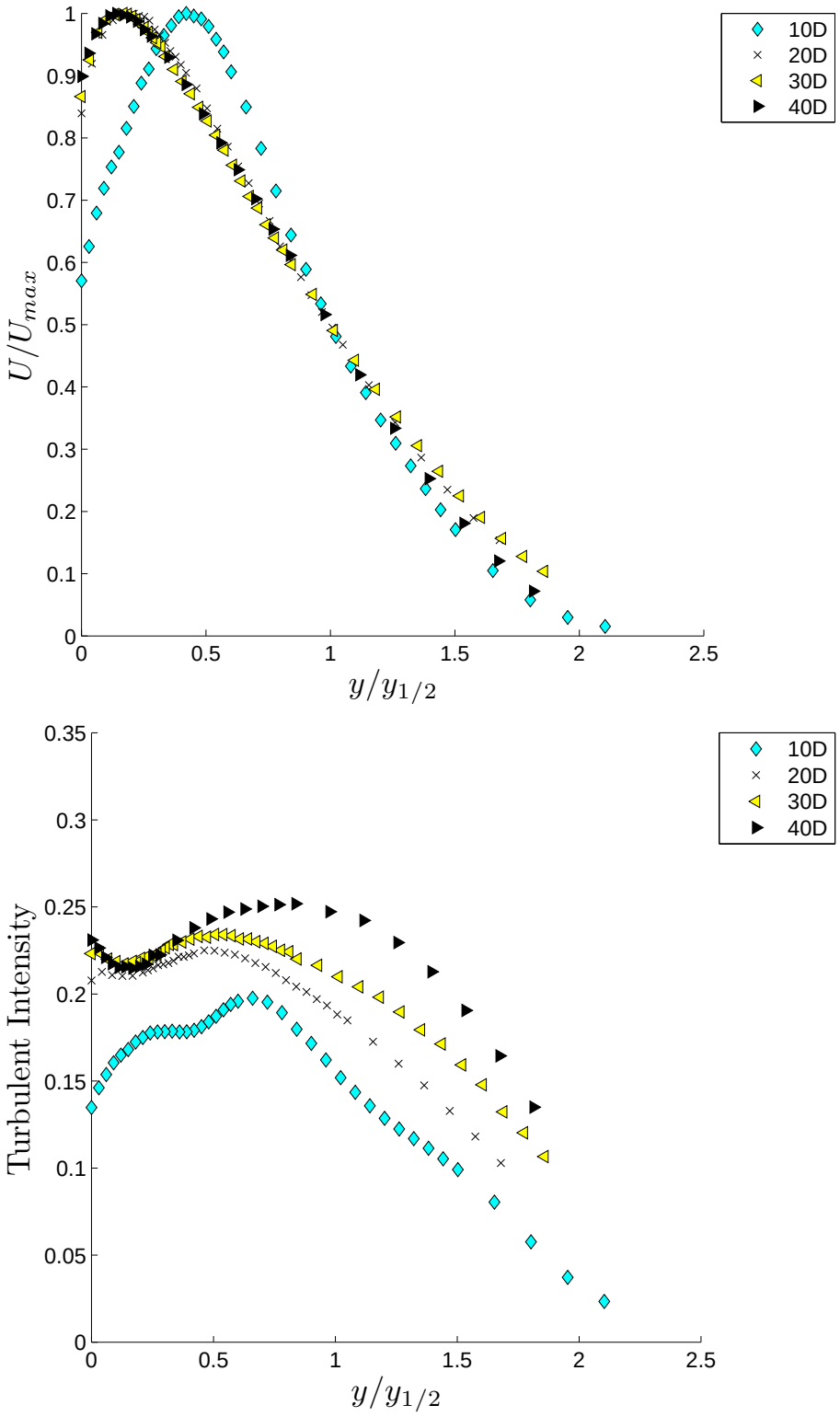

Figure 4.5: Profiles of the mean (top) and turbulent intensity (bottom) measured on the jet centreline in the intermediate to far-field region normalized in terms of similarity variables.

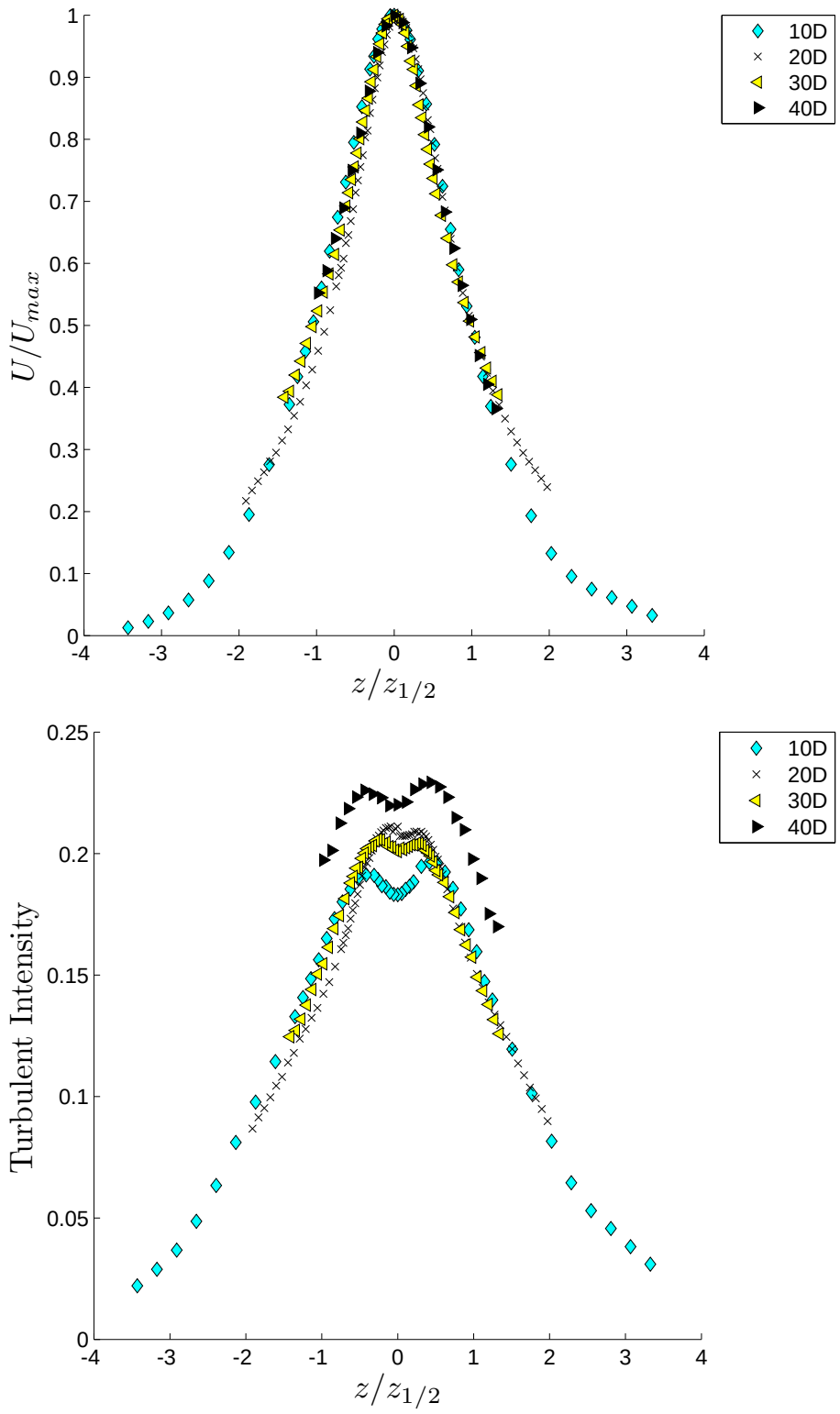

Figure 4.6: Profiles of the mean (top) and turbulent velocity (bottom) measured across the jet at y_{max} in the intermediate to far-field region normalized in terms of similarity variables..

normalized by so-called similarity variables, the local maximum flow velocity and the respective jet half-width. The collapse of the mean profiles indicate that the mean flow is becoming self similar at $\frac{x}{D} = 20$. The turbulent profiles, however tend to approach a self similar state more slowly, as expected. The turbulence profile at $\frac{x}{D} = 20$ and 30 exhibit the classical wall jet behavior with an outer peak associated with jet-like shearing of the ambient air and a second peak associated with turbulent production near the wall. Sun et al [2] for example, showed that turbulent profiles generally become self-similar, at $\frac{x}{D} = 50$ and beyond, this is consistent with the findings here. The mean and turbulent profiles measured across the jet at $\frac{x}{D} = 10$ to 40 are shown in figure 4.6, scaled using the same similarity variables. The mean profiles collapse while again the turbulence profiles are slower to collapse, for the same reasons as discussed previously.

4.2 The Corner Wall Jet

The approach to investigating the corner wall jet was different then the wall jet or free jet. Rather than characterizing the jet using only two profiles, the corner wall jet was analyzed by performing measurements on a sixteen by sixteen grid, for 256 velocity measurements at each streamwise position. The measurements were performed in the corner jet from the jet outlet to $40D$ downstream.

In figure's 4.7 to 4.11, the mean velocity contours at each downstream location are shown along with the respective streamwise turbulent velocity contours. The coordinates are normalized by D and both velocities are normalized by U_{max}. The reader is reminded that the z and y axis represent the location of the two walls in the corner wall jet.

Figure 4.7 shows the contours for the corner wall jet just as it is exiting out the pipe. For the most part, the flow is unaffected by the wall as both the mean and turbulence contours are still round. The mean contours appear concentrated at the center of the pipe due to the shape of the profiles for fully developed turbulent pipe flow. The turbulence contours show the highest levels in a circular region in the center of the pipe which are around 5%, these levels are consistent with the profile measurements shown earlier.

Examining the contours further downstream at $\frac{x}{D} = 10$ (figure 4.8), the flow can be observed to be starting to develop as the mean flow contours begin to distort near the wall. This behavior is not unlike that observed in the near-field of a three-dimensional wall jet by Hall and Ewing [19]. The core of the jet, though, remains quite round, still showing remnants of the initial pipe flow. The turbulence intensity is the largest at the core of the wall jet; this is consistent with previous contours of the velocity field at this streamwise position in the three-dimensional wall jet by Hall and Ewing [19]. The contours levels indicate that the turbulent intensity at the core of the corner wall jet here approaches 20%. Interestingly, this is quite similar

to the peak values measured earlier in the three-dimensional wall jet (figure 4.1) .

Further downstream at $\frac{x}{D} = 20$ and 30, as shown in figure 4.9 and 4.10 respectively, the mean contours continue to develop along the walls. The region of highest velocity remains reasonably circular and stays near the wall at the corner, the largest streamwise turbulence levels also correspond to this same region. Contour plots at $40D$ (figure 4.11) have a similar shape but are even wider, expanding along the wall. The mean contours at $\frac{x}{D} = 40$ appear quite similar to those of Hogg and Launder's [6] at $\frac{x}{D} = 50$. At $\frac{x}{D} = 40$, the turbulent contours have a large core region that exceeds 20% turbulence intensity; this value is comparable to the turbulence intensities measured in the three-dimensional wall jet at this position. This suggests that, despite the differences between the two geometries, the mixing is likely comparable in the two flows.

Mean and turbulent velocity profiles taken along the corner bisector, a 45° line that starts at the origin of the corner, are shown in the near-field in figure 4.12. These plots are analogous to the standard three-dimensional wall jet profiles taken at the centerline with regards to symmetry. At $\frac{x}{D} = 0$, the pipe flow profile is visible in the mean flow contours and two peaks associated with fully developed pipe flow are shown in the turbulence intensity profile. Further downstream the mean flow profiles begin to grow outward and the inner peak in the turbulence intensity profile is overwhelmed by a single larger outer peak, likely due to the shearing of the jet with the quiescent air as it moves downstream.

Similar profiles along the bisector, this time in the intermediate field, are shown in figure 4.13. Here, the coordinates are again normalized by the pipe diameter, D. The mean flow continues to evolve and produces a profile that resembles a classical wall jet. The turbulence intensity again shows one dominant peak which reaches values of approximately 22%, similar to that measured in the three-dimensional wall jet.

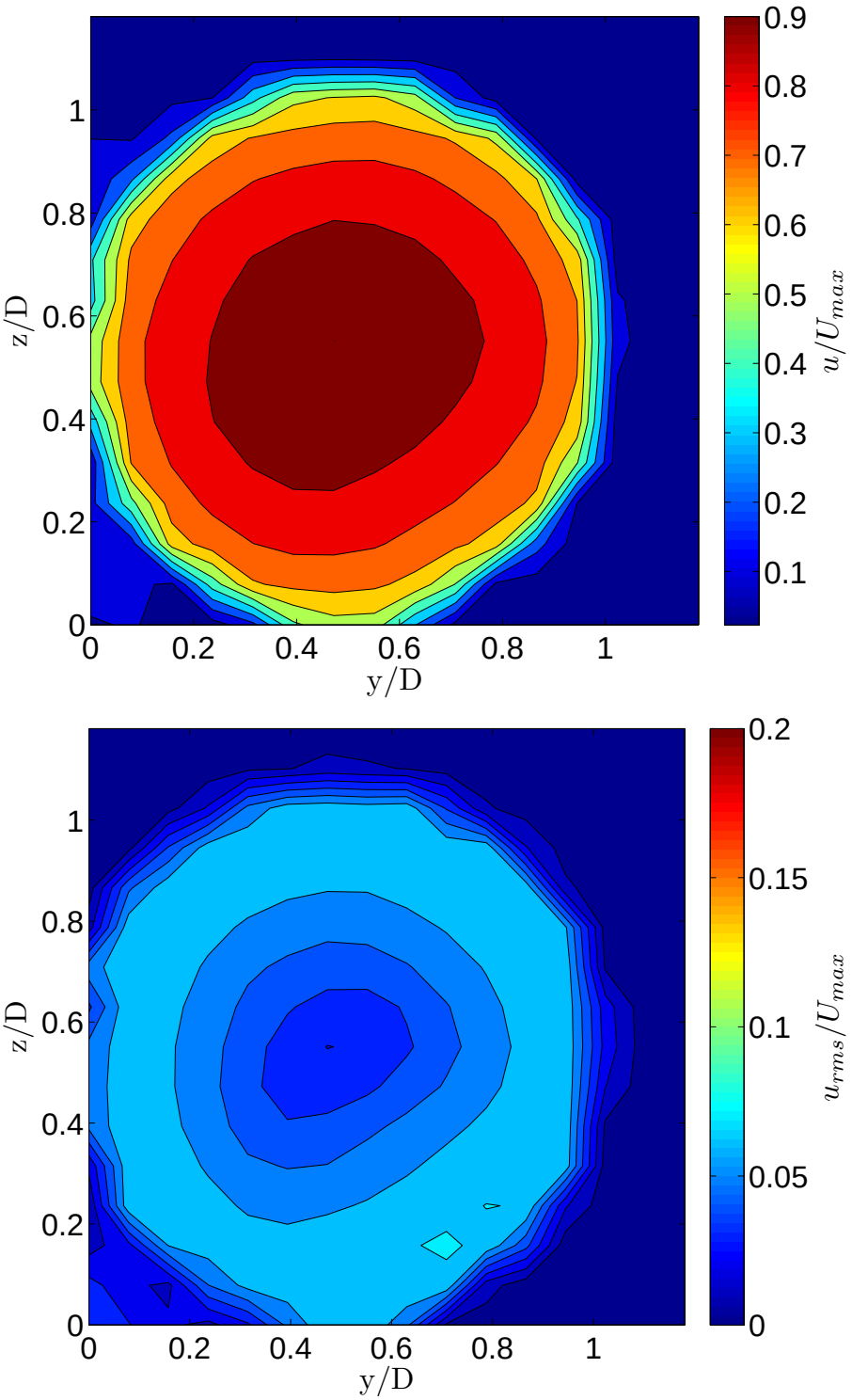

Figure 4.7: Mean velocity (top) and turbulent intensity (bottom) contours measured in a corner wall jet at the jet outlet, $\frac{x}{D} = 0$.

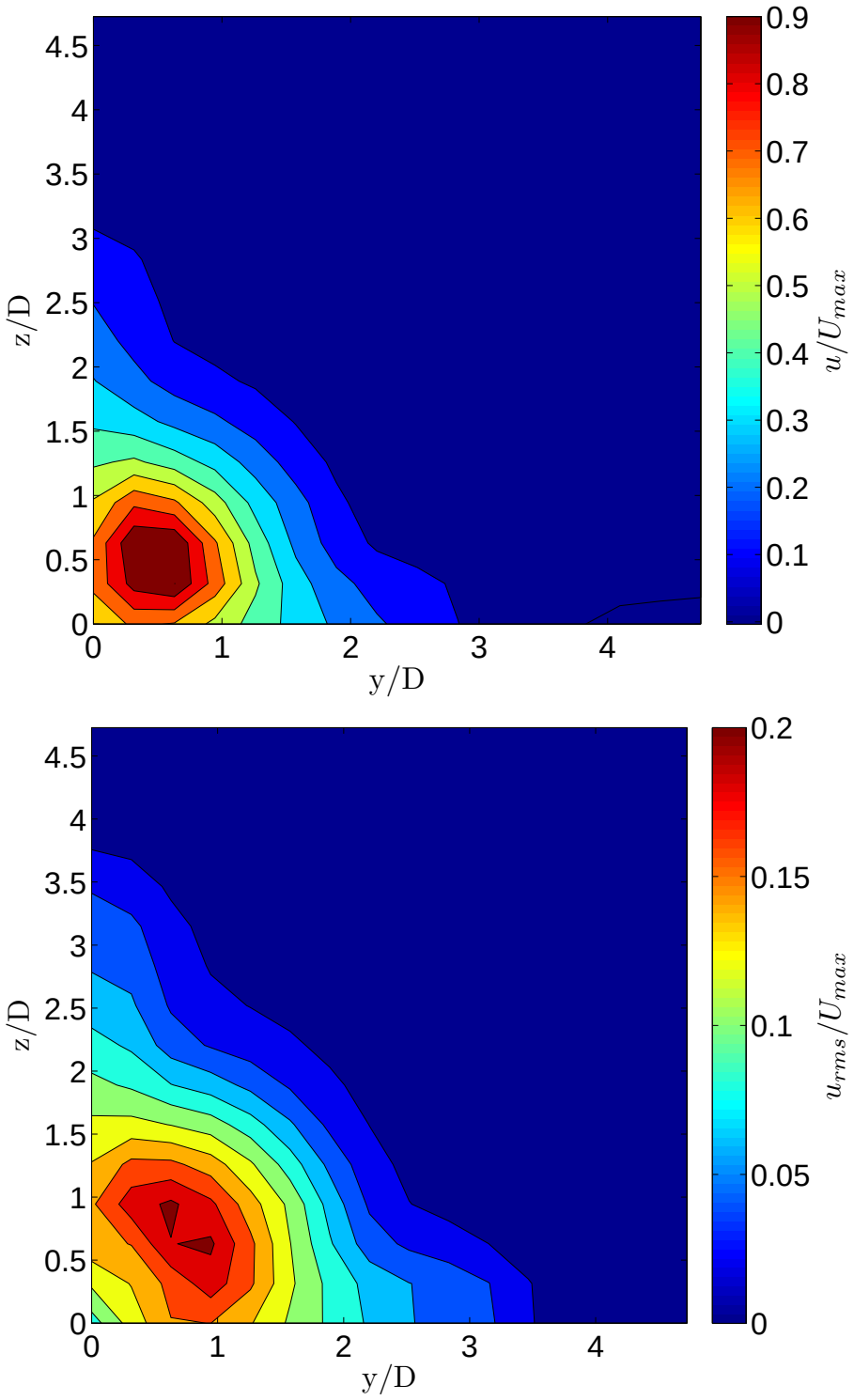

Figure 4.8: Mean velocity (top) and turbulent intensity (bottom) contours measured in a corner wall jet at $\frac{x}{D} = 10$.

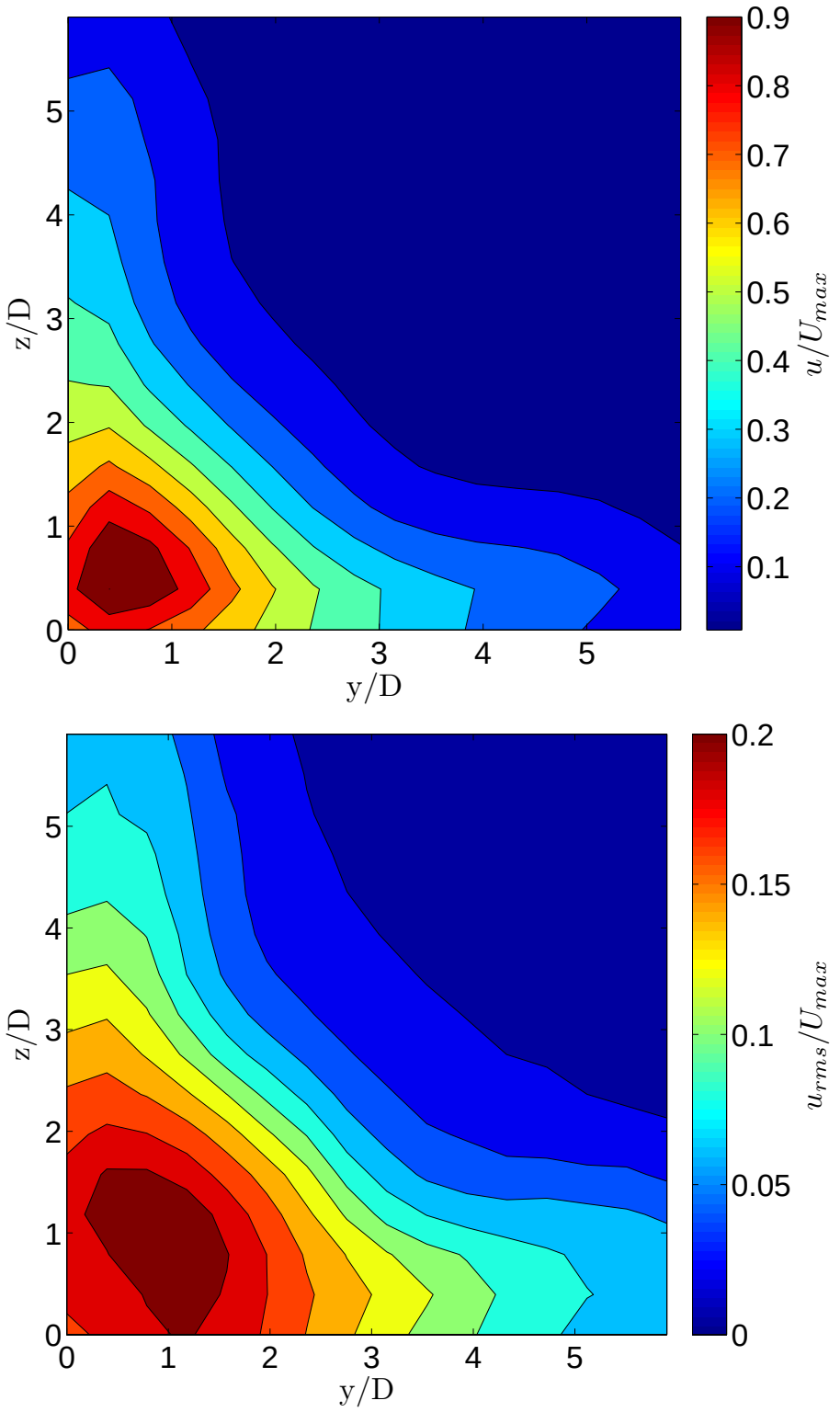

Figure 4.9: Mean velocity (top) and turbulent intensity (bottom) contours measured in a corner wall jet at $\frac{x}{D} = 20$.

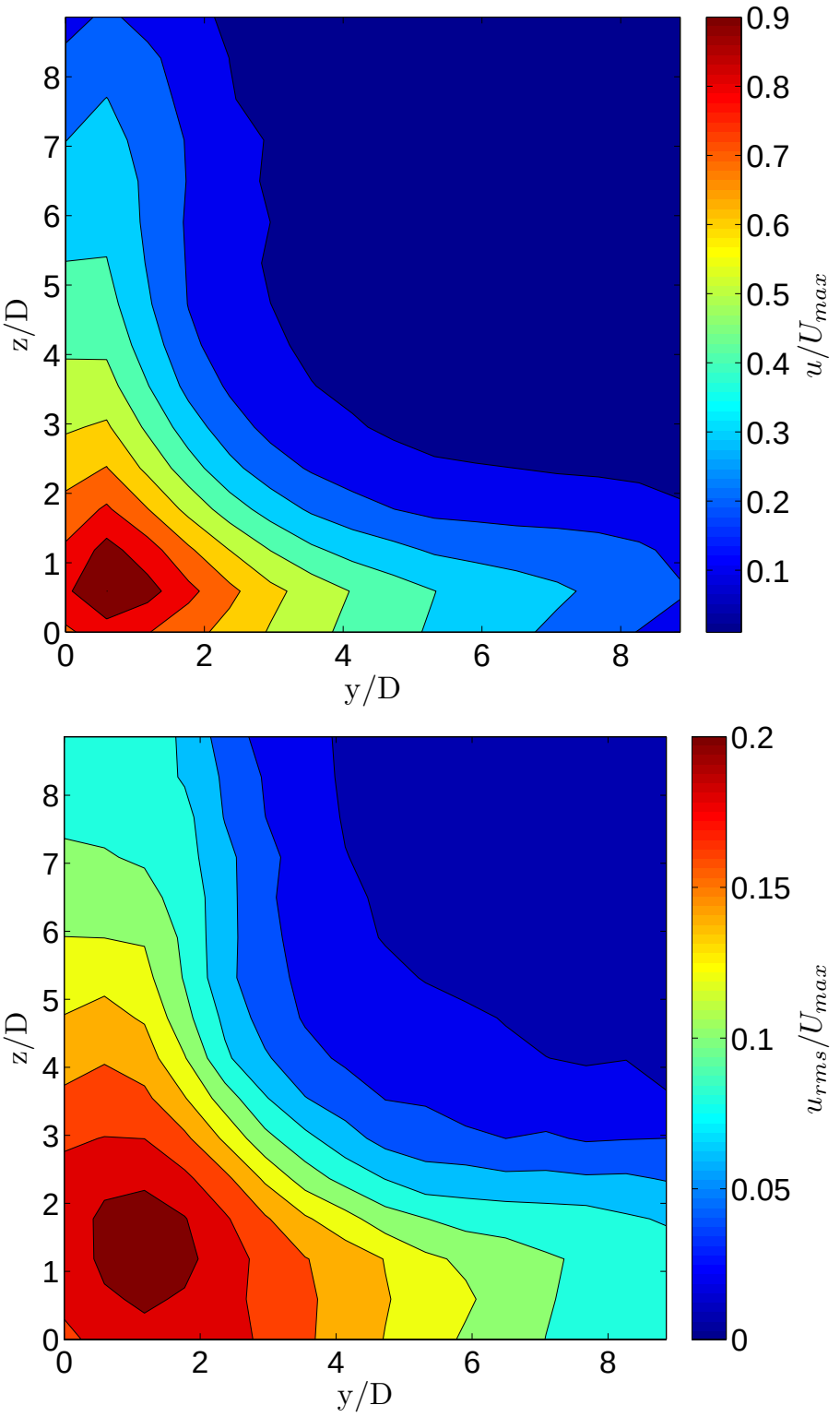

Figure 4.10: Mean velocity (top) and turbulent intensity (bottom) contours measured in a corner wall jet at $\frac{x}{D} = 30$.

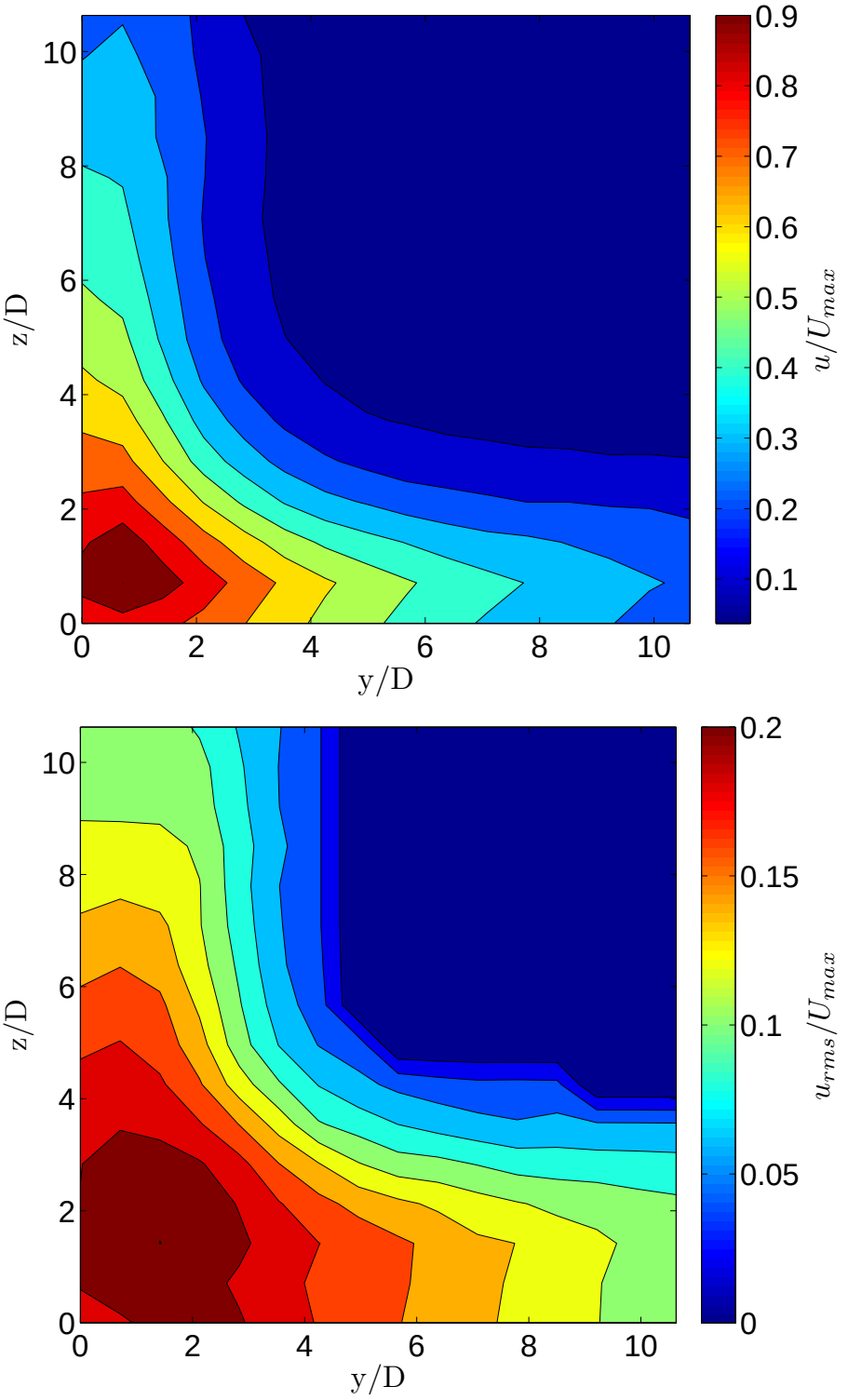

Figure 4.11: Mean velocity (top) and turbulent intensity (bottom) contours measured in a corner wall jet at $\frac{x}{D} = 40$.

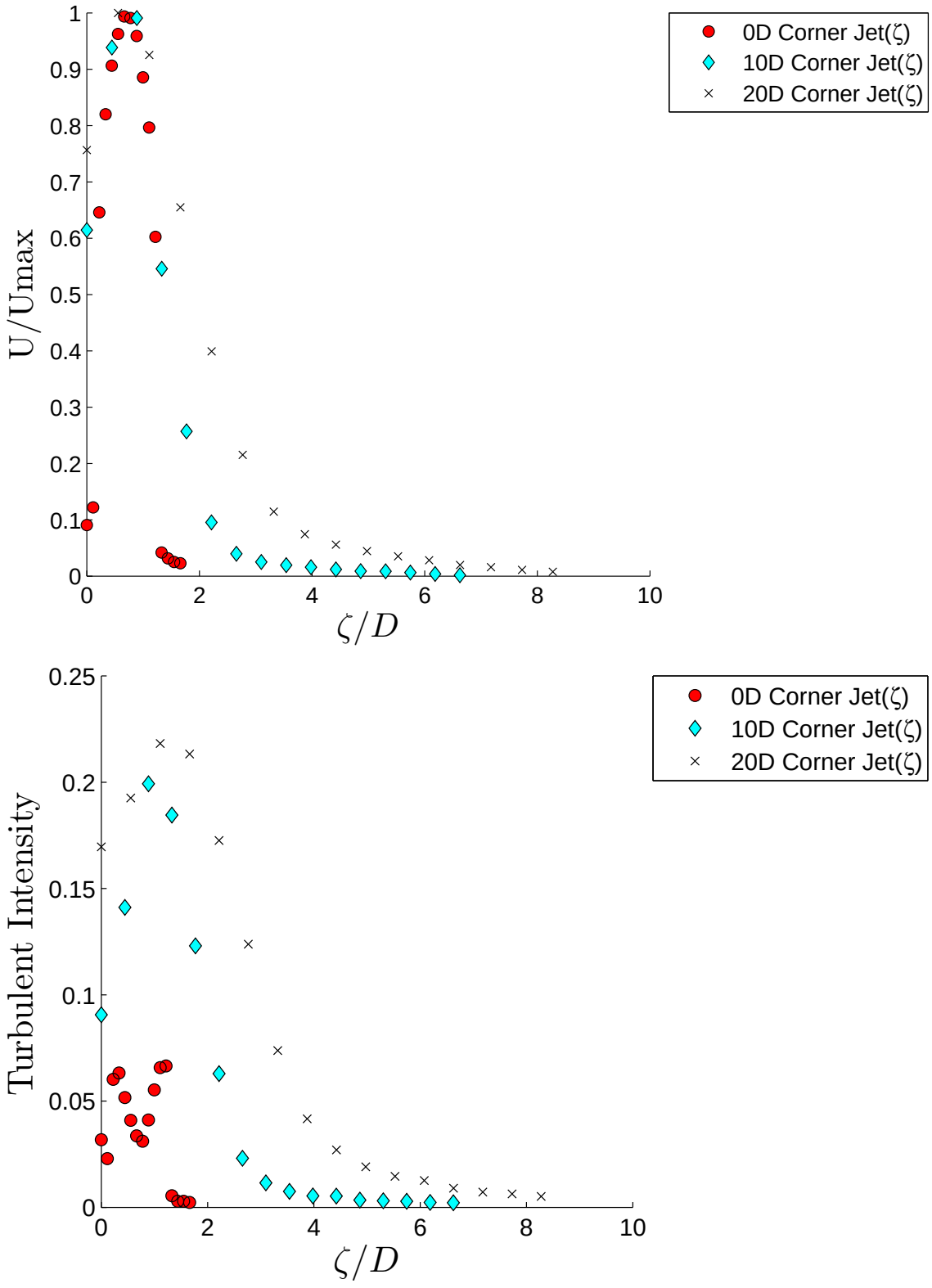

Figure 4.12: Mean velocity (top) and turbulent intensity (bottom) bisector profiles in the near-field of a corner wall jet.

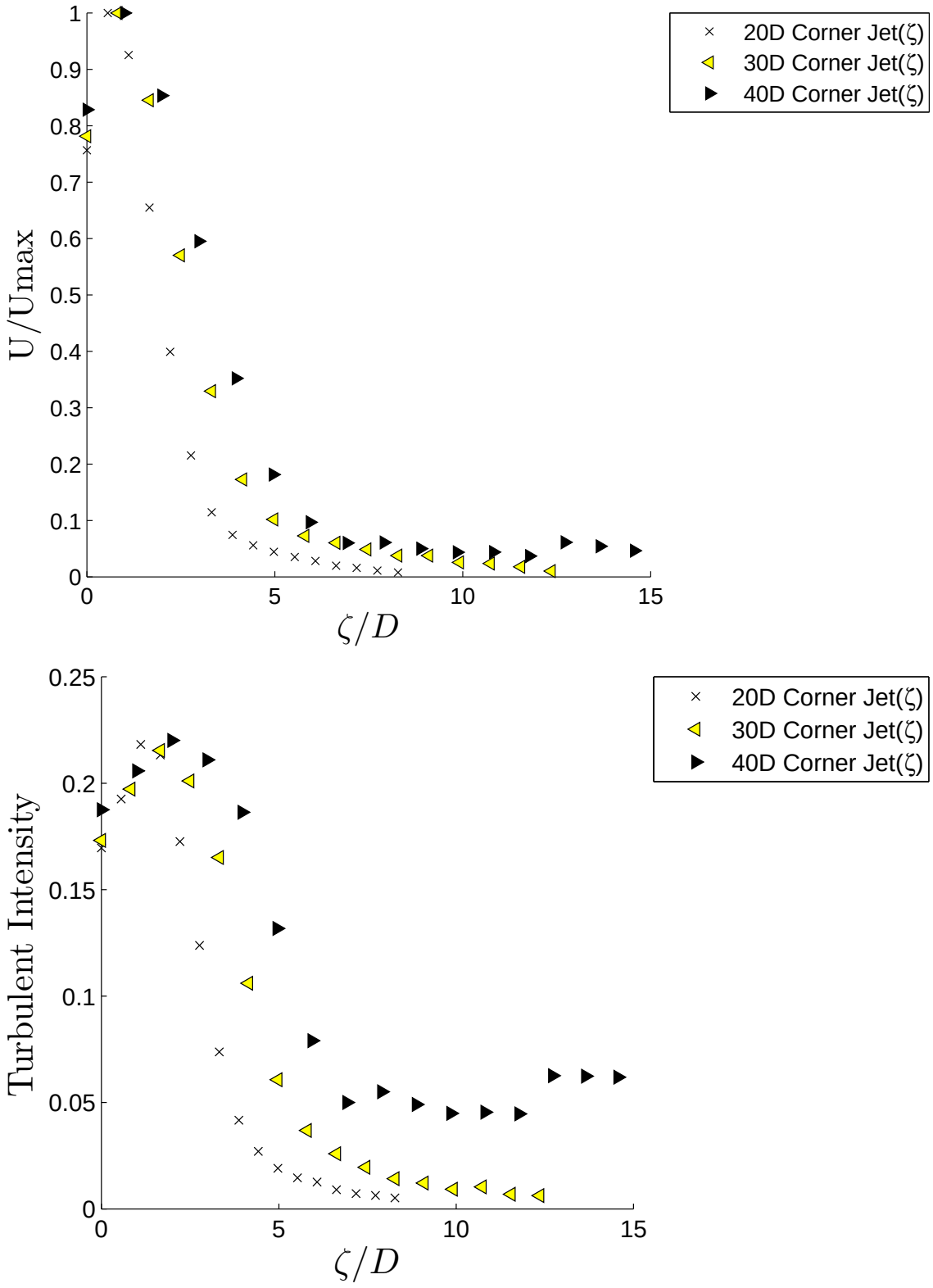

Figure 4.13: Mean velocity (top) and turbulent intensity (bottom) bisector profiles in the intermediate field of a corner wall jet.

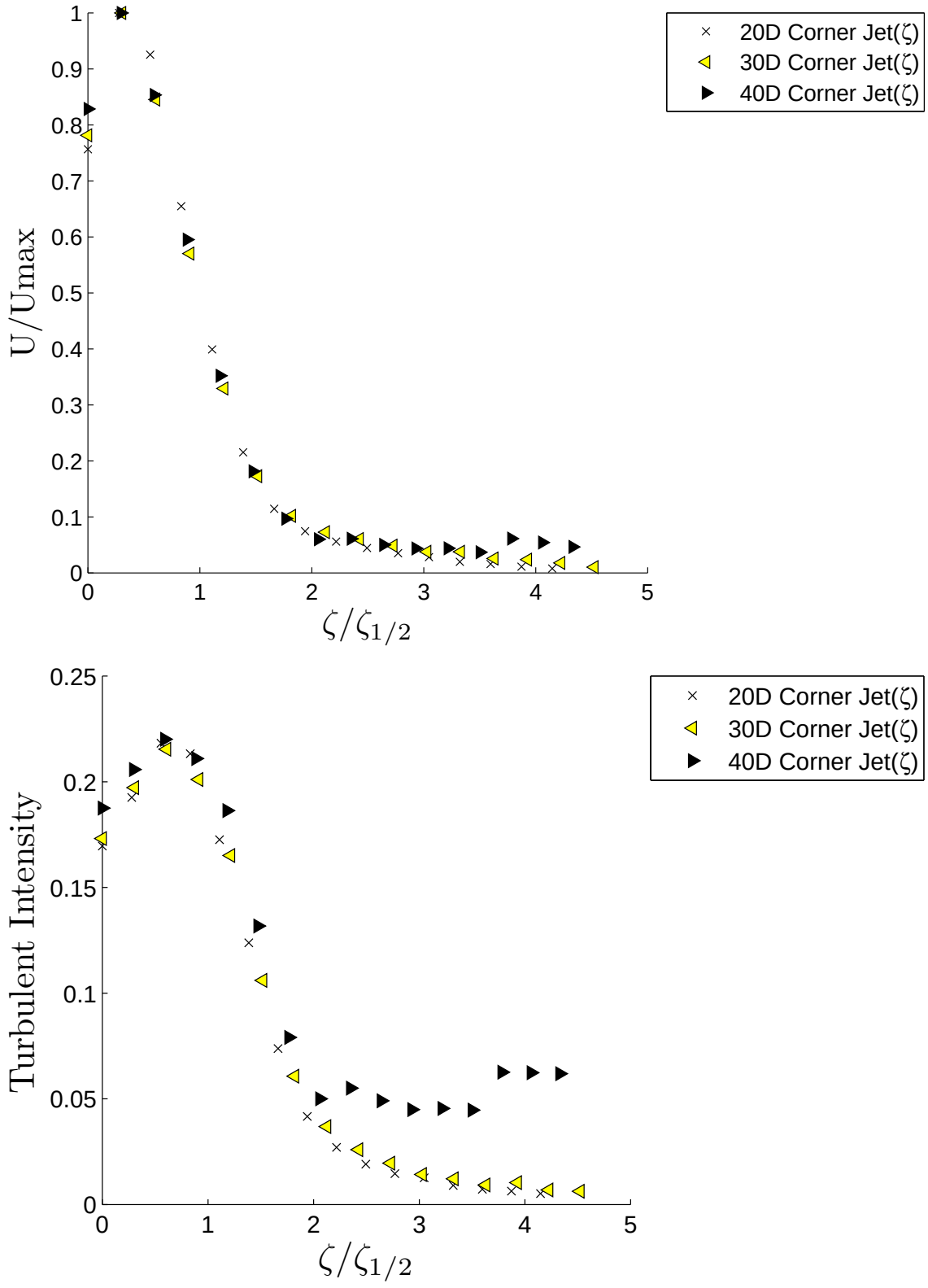

Figure 4.14: Mean velocity (top) and turbulent intensity (bottom) bisector profiles normalized in terms of similarity variables in the intermediate field of a corner wall jet.

The bisector profiles in the intermediate field are re-plotted in figure 4.14, however, in this case, the bisector coordinate is normalized by the bisector half-width at each downstream position. The bisector half-width was determined by inspection from the bisector velocity profiles. The collapse of both the mean and turbulence profiles here indicates that the flow is approaching the self preserving state when examined from the perspective of the bisector axis.

To further assess whether the flow in the corner wall jet is truly evolving towards a self-similar state, contours of the mean streamwise velocity are shown at $\frac{x}{D} = 30$ and 40 in figure 4.15. In this case, the contours have been normalized by $y_{\frac{1}{2}}$ and $z_{\frac{1}{2}}$. In both cases the contours of mean velocity are, for the most part, quite similar. There are however some small differences in the contours, for example, the high velocity core of the jet seems to persist closer to the wall for the $\frac{x}{D} = 40$ case. This suggests that the mean flow is tending towards self-similarity, but has not quite been reached in these measurements. This is not surprising as it is well known that it takes roughly 40 or 50 diameters before the mean flow in the three-dimensional wall jet becomes self-similar [9, 23, 2]. This also indicates the measurements taken along on the bisector may not be truly indicative of full flow similarity. This is further confirmed upon inspection of the contours of turbulence intensity where the coordinates are normalized by the half-widths (figure 4.16). Again, the contours are reasonably similar but there are small differences between the two jets, particularly at the core of the jet, near the vertex of the corner.

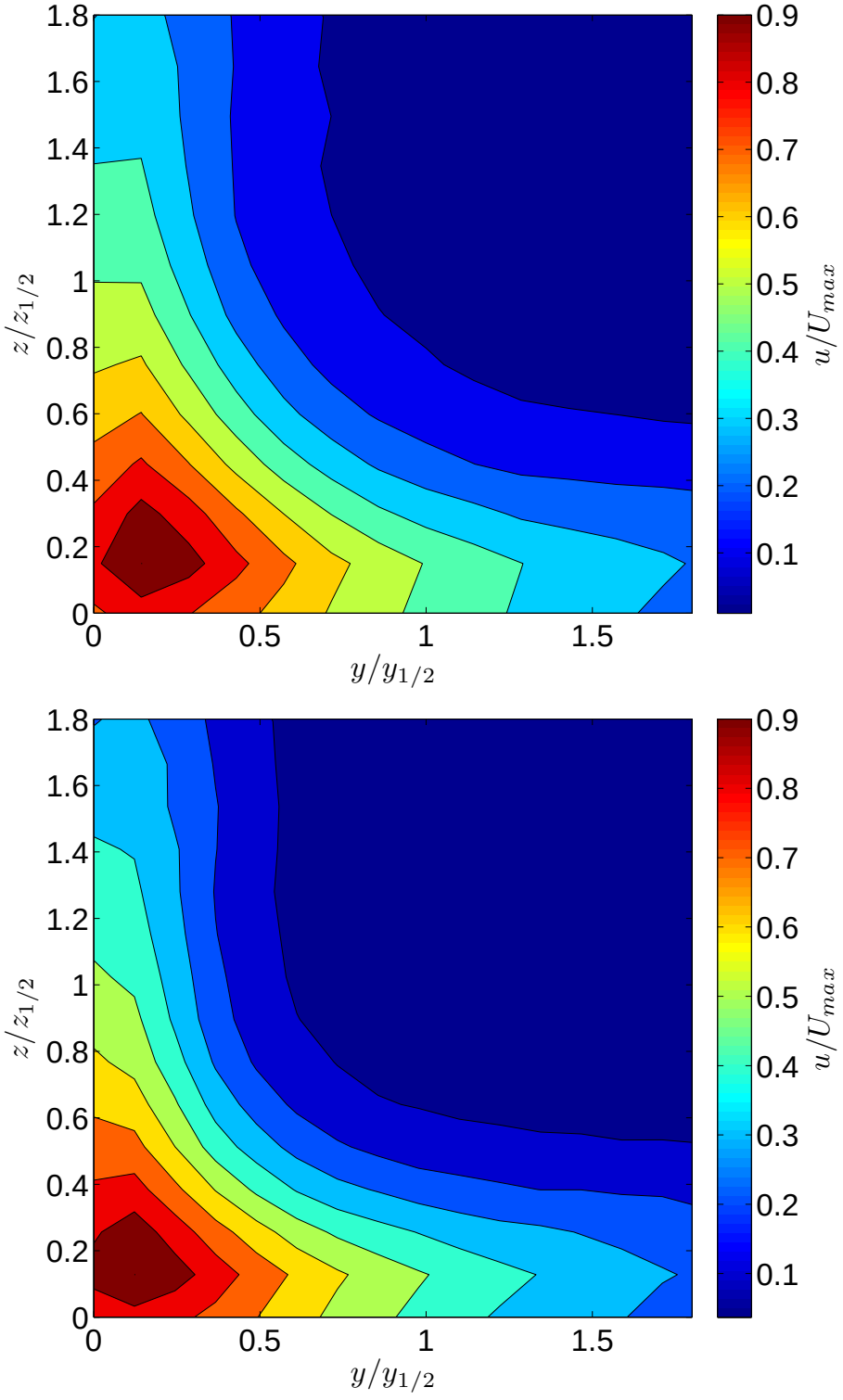

Figure 4.15: Mean velocity contours normalized in similarity variables at $\frac{x}{D} = 30$ (top) and $\frac{x}{D} = 40$ (bottom).

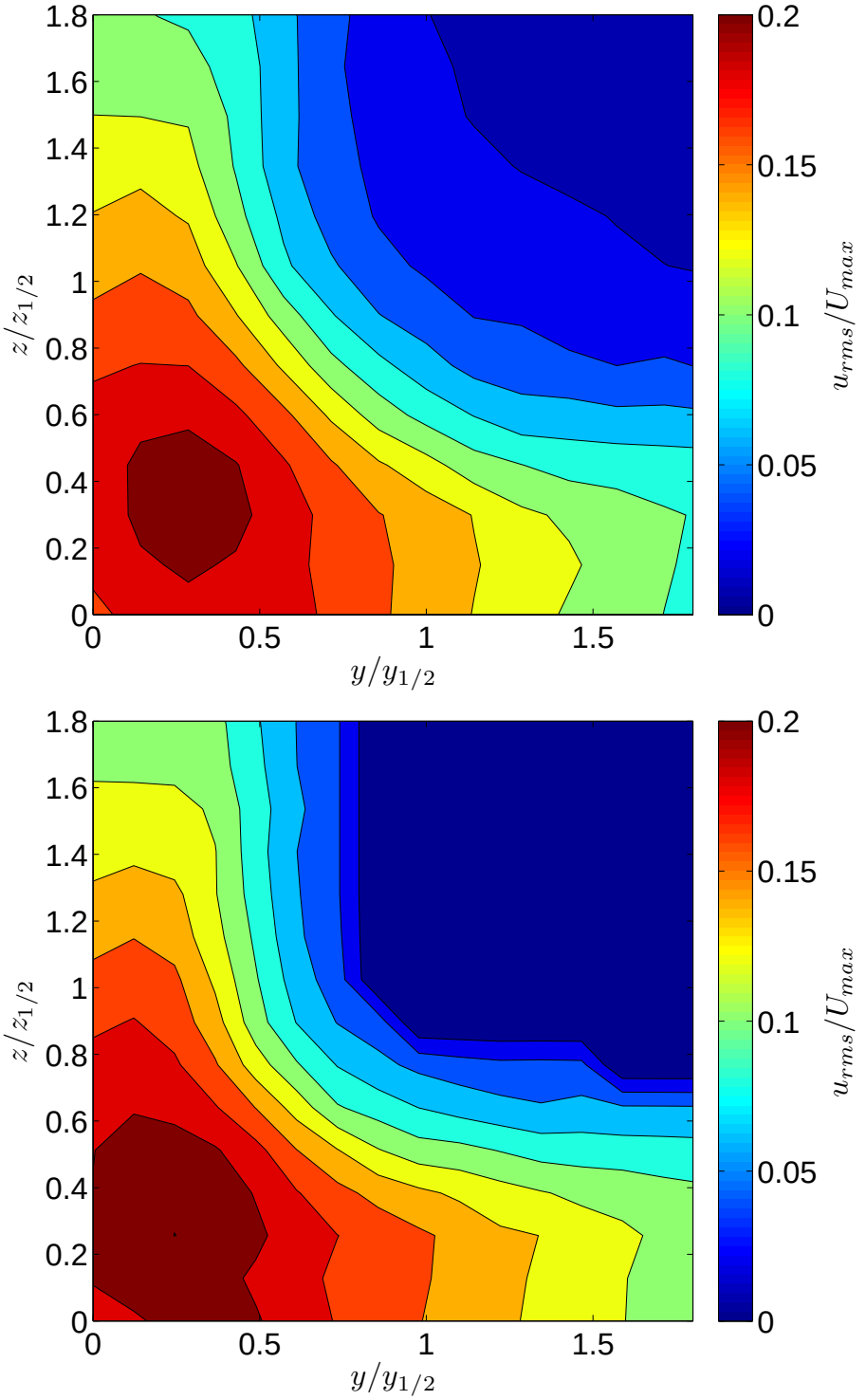

Figure 4.16: Contours of turbulence intensity normalized in similarity variables at $\frac{x}{D} = 30$ (top) and $\frac{x}{D} = 40$ (bottom).

4.3 Discussion: Comparison of the Wall Jet with Corner Wall Jet

The streamwise decay of the maximum velocity point in the three-dimensional wall jet is compared to the corner wall jets in figure 4.17. When the values of the three-dimensional wall jet are compared at $\frac{x}{D} = 10$ to the values obtained in the corner wall jet at the same position, they are shown to be quite similar. Further downstream at $\frac{x}{D} = 30$ to 40, the maximum velocity is higher in the corner wall jet, this indicates that the corner wall jet develops slightly slower than the three-dimensional wall jet. However by $\frac{x}{D} = 40$ the differences between the two jets are quite small.

In figure 4.18, both the $y_{\frac{1}{2}(//)}$ and $z_{\frac{1}{2}(//)}$ half-widths in the corner wall jet are compared to the half-widths in the three-dimensional wall jet. For the corner wall jet, there are only very small differences in the values of $y_{\frac{1}{2}(//)}$ and $z_{\frac{1}{2}(//)}$ indicating the jet is developing symmetrically, as expected. Here, the bisector maximum velocity point, ζ_m, is used to define the height of the corner wall jet. For the corner wall jet, the $y_{\frac{1}{2}}$, $z_{\frac{1}{2}}$ and the $\zeta_{\frac{1}{2}}$ are all comparable at $\frac{x}{D} = 10$. As the corner jet develops further downstream to $\frac{x}{D} = 20$, the values of $y_{\frac{1}{2}(//)}$ and $z_{\frac{1}{2}(//)}$ are considerably larger than the bisector half width (2 as compared to 2.5). Further downstream, the half-widths for the corner wall jet all grow reasonably linearly until $\frac{x}{D} = 40$.

At $\frac{x}{D} = 10$ and 20, the three-dimensional wall jet vertical half-width, $y_{\frac{1}{2}}$ is comparable to the $\zeta_{\frac{1}{2}}$ for the corner wall jet. However, by $\frac{x}{D} = 30$, the $\zeta_{\frac{1}{2}}$ for the corner wall jet is larger than that of the three-dimensional wall jet. This is no doubt related to the development of the lateral half-widths parallel to the wall in both jets. In particular, the values of $y_{\frac{1}{2}(//)}$ and $z_{\frac{1}{2}(//)}$ in the corner wall jet are, somewhat surprisingly, larger than the lateral half-width in the three-dimensional wall jet at $\frac{x}{D} = 10$. By $\frac{x}{D} = 20$, the lateral half-width in the three-dimensional wall jet has slightly surpassed the corner wall jet. By $\frac{x}{D} = 30$ and 40, the three-dimensional wall

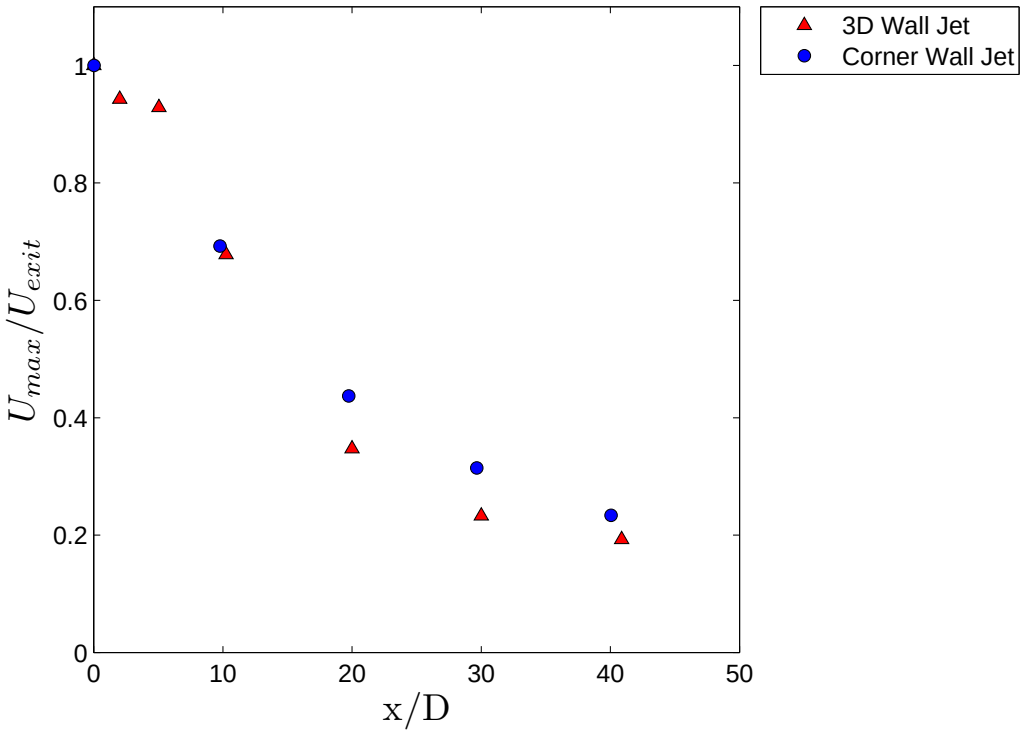

Figure 4.17: A comparison of the streamwise decay of the local maximum mean velocity for the three-dimensional wall jet and the corner wall jet.

jet is significantly wider than the corner wall jet.

At $\frac{x}{D} = 40$, the lateral half-width for the three-dimensional wall jet is approximately 2.6 times larger than the half-width measured normal to the wall. whereas in the corner wall jet, the lateral half-width is only 2.1 times larger than the bisector half-width. This suggests that the secondary flow, and likely the turbulent generated secondary flow is weaker in the corner wall jet than in the three-dimensional wall jet. As the velocity decay suggests that the differences are small by $\frac{x}{D} = 40$, it is not likely that these differences can be attributed to the corner wall jet development being delayed.

The growth rates from figure 4.18 are summarized in table 4.1 in the far-field for the corner wall jet and the three-dimensional jet. It can b e observed that the growth rate of the three-dimensional wall jet is slightly larger than for the corner wall jet in the lateral direction ($\frac{\partial z_{\frac{1}{2}}}{\partial x}$), parallel to the wall, 0.18 verses 0.16, respectively. The

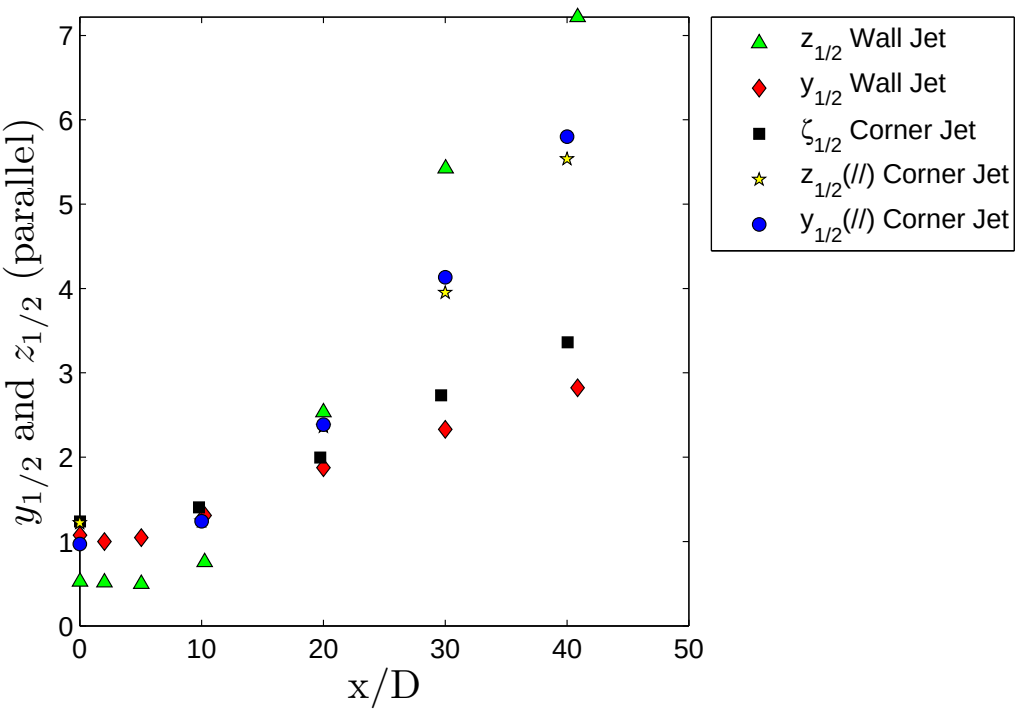

Figure 4.18: A comparison of the streamwise growth of the jet half-widths in the three-dimensional wall jet and the corner wall jet.

growth rates along the jet centreline for the three-dimensional wall jet ($\frac{\partial y_{\frac{1}{2}}}{\partial x}$) is 0.05, whereas for the corner jet ($\frac{\partial \zeta_{\frac{1}{2}}}{\partial x}$) the value is slightly larger at 0.06. To compare the disparity in the growth rates of the two jets further, the ratio of lateral to vertical growth rates is examined, $\frac{\partial y_{\frac{1}{2}}/\partial x}{\partial z_{\frac{1}{2}}/\partial x}$ and $\frac{\partial \zeta_{\frac{1}{2}}}{\partial y_{\frac{1}{2}}}$, respectively, give ratios of 3.65 for the wall jet and 2.64 for the corner wall jet. Thus, the corner wall jet has a smaller disparity in the growth rates than the 3D wall jet. This indicates that there are differences in the strength of the secondary flow in the two jets.

The mean velocity profiles measured on the centreline of the three-dimensional wall jet profiles are directly compared to profiles measured on the corner wall jet in figure 4.19. As the growth of the two flows have been demonstrated to be different, the profiles are normalized in similarity coordinates and are shown in the intermediate field. Although there is considerably more data for the three-dimensional wall jet

Table 4.1: Summary of three-dimensional wall jet and corner jet investigation in the far-field.

Jet Investigated	Region ($\frac{x}{D}$)	Growth Rate	Value
3D Wall Jet	$30-40$ (Far Field)	$\frac{\partial y_{\frac{1}{2}}}{\partial x}$	0.05
		$\frac{\partial z_{\frac{1}{2}}}{\partial x}$	0.18
		$\frac{\partial y_{\frac{1}{2}}/\partial x}{\partial z_{\frac{1}{2}}/\partial x}$	3.65
Corner Wall Jet	$30-40$ (Far Field)	$\frac{\partial \zeta_{\frac{1}{2}}}{\partial x}$	0.06
		$\frac{\partial z_{\frac{1}{2}}}{\partial x}$	0.16
		$\frac{\partial \zeta_{\frac{1}{2}}}{\partial y_{\frac{1}{2}}}$	2.64

than the corner wall jet[1], it is apparent that the profiles in the corner wall jet have a similar shape to the three-dimensional wall jet profiles at both of the depicted positions. This indicates that the corner wall is behaving *loosely* like a three-dimensional wall jet, at least on the centreline, despite the different wall orientations used here.

[1]This is obviously a result of the corner wall jet measurements being performed on a 16x16 grid to capture both sides of the flow.

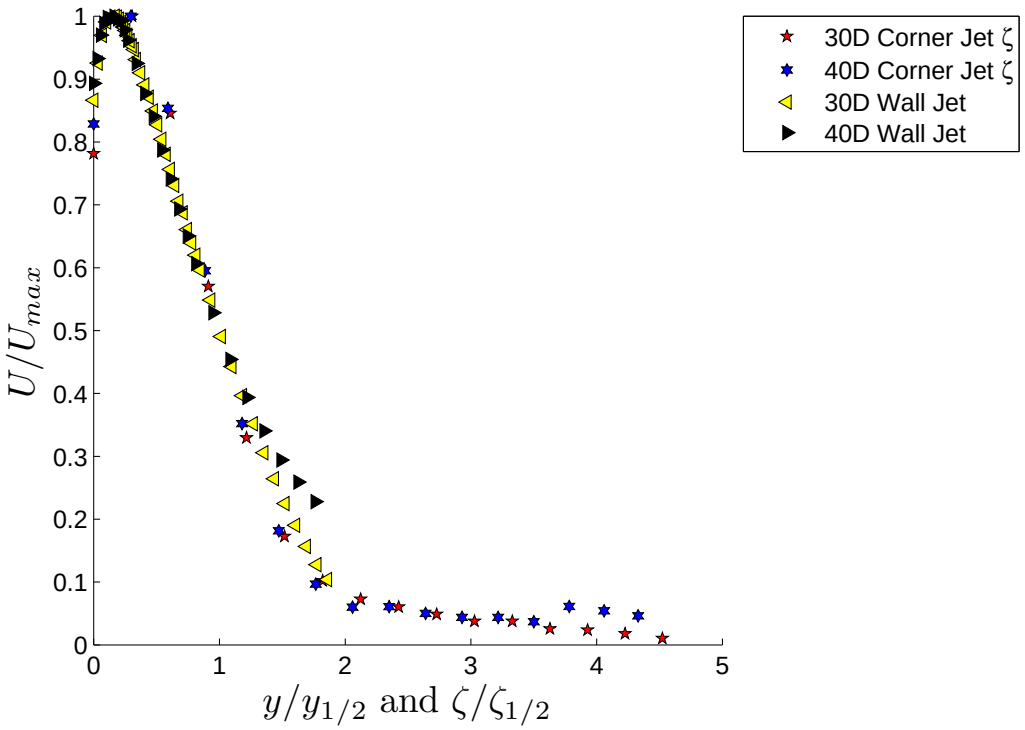

Figure 4.19: Bisector mean velocity profiles in the corner jet compared to three-dimensional wall jet profiles measured normal to the wall.

Chapter 5

Conclusion and Recommendations for Future Work

5.1 Conclusions

An experimental facility was designed, built and commissioned to allow the conventional turbulent wall jet and the corner wall jet to be studied. Hot-wire measurements were performed in a three-dimensional wall jet formed using a long round pipe and in a corner wall jet formed with a long round pipe. Profiles were measured in the first case and full flow field measurements were performed in the later case. Both mean and turbulent profiles and contours were examined and compared for both jets. Although the mean flow was previously studied by Hogg and Launder[6] in the far-field, these measurements represent the first measurements of the mean and turbulent velocity in the the corner wall jet in the near and intermediate field (40 diameters and lower). A number of significant findings came out of this work:

- The corner wall jet bisector profiles look quite similar to profiles measured in a three-dimensional wall jet, particularly in the near-field and when normalized using similarity coordinates. This indicates that the corner jet still behaves in

general, like a wall jet.

- The flow in the corner wall jet grows much more rapidly parallel to the wall than along the centreline, not unlike the turbulent three-dimensional wall jet. However, the corner wall jet does not grow quite as rapidly, parallel to the wall, and grows significantly slower along the bisector. This suggests that there must be differences in the secondary flow of the two jets. Speculatively, this could be tied to difference in entrainment caused by the orientation of the walls for the corner wall jet.

- The maximum velocity point decays slightly slower in the corner wall jet than the three-dimensional wall jet, but is comparable by $\frac{x}{D} = 40$ to the wall jet. This indicates that the lower growth rate of the corner wall jet in contrast to the three-dimensional wall jet is not simply due to the delayed development of the corner wall jet.

- The mean and turbulent velocities measured on the bisector of the corner jet approach self-similarity by $\frac{x}{D} = 30$ to 40. This was not true for the full flow field which indicates that the jet is still approaching similarity at these positions. This also indicates that measurements on the corner bisector are not necessarily representative of full flow field similarity.

5.2 Recommendations for Future Work

It would be useful to have measurements in the corner wall jet past $x/D = 40$ and well into the jet far-field. In order to do this, the current experimental facility would need to be modified or rebuilt. In particular, the corner wall jet facility could be made larger so the full streamwise development of the jet from the exit to at least $60D$ could be ascertained. This would have the added benefit of allowing for PIV and hotwire measurements could also be made on the same facility. These new experiments would help to confirm the findings in the present work regarding growth rates between the corner jet and wall jet to see if they are actually in the far-field.

The measurement procedures should be modified to increase the resolution of the available space during corner jet profile experiments from it's current maximum of a 16 by 16 grid to a higher resolution, particularly near the wall. This addition would not only improve existing comparisons but would also allow the corner jet data to be better resolved in order to determine the mass entrainment and momentum flux in the corner wall jet. It is recommend that in order to increase the resolution beyond the 16 by 16 grid, the measurements be assisted by automation. Just doubling the resolution to a 32 by 32 grid at a minimum of one to two minutes per point gives approximately 17 hours of measurements straight for a single profile of the corner wall jet using hotwire anemometry. A way to reduce this time would be to cut the data space in half and assume that the corner jet is symmetrical about the bisector axis ζ; this would only take half as much time and still be possible to complete a set of data in a single experiment.

The present facility could be modified to examine a heretofore unexplored flow, a so-called "obtuse jet". An example of this is shown in figure 5.1. The obtuse just is an intermediary between the flat wall jet and the corner wall jet, meaning that it would probably be similar to the corner wall jet only the vertical wall would be set at 135° instead of 90°. Measurements in this flow could reveal more insight into how

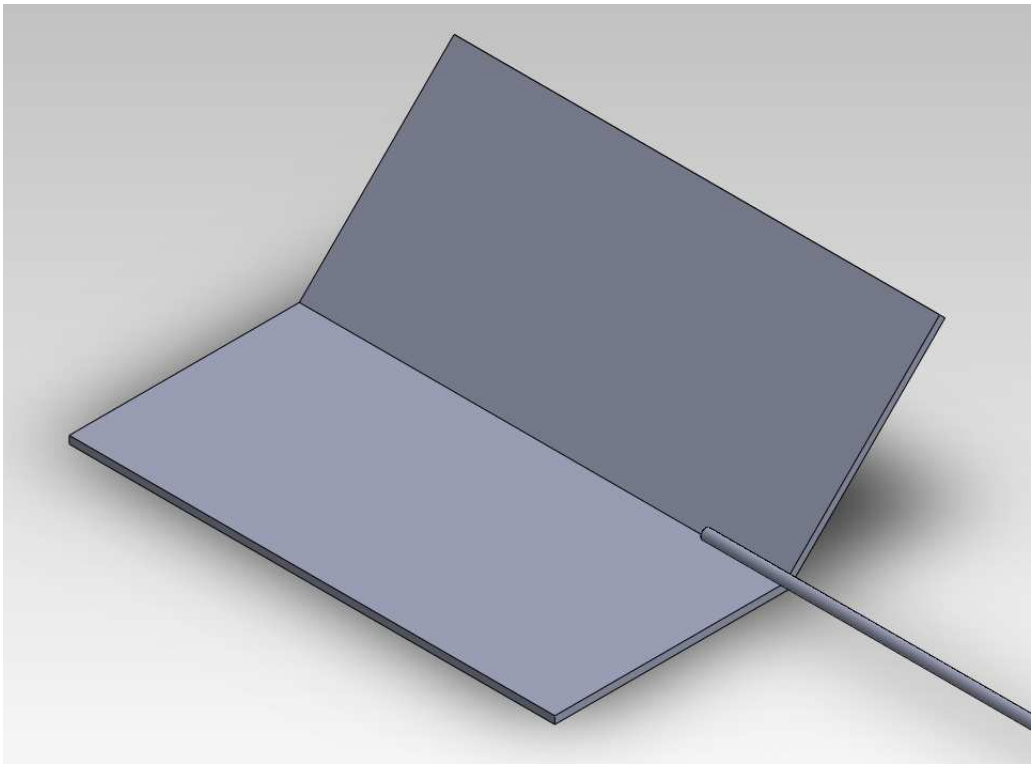

Figure 5.1: Schematic of obtuse wall jet.

a jet develops along a corner.

Bibliography

[1] J. W. Hall. *The Role of the Large-Scale Structures in the Development of Turbulent Wall Jets*. PhD thesis, McMaster University, Mechanical Engineering,, Hamilton, 2005.

[2] H. Sun. *Development of Three-Dimensional Turbulent Wall Jets*. PhD thesis, Mechanical Engineering, McMaster University, Hamilton, 2002.

[3] M. R. Davis and H. Winarto. Jet diffusion from a circular nozzle above a solid plane. *Journal of Fluid Mechanics*, (101 pt 1):201–221, 1980.

[4] F.B. Gessner and J.B. Jones. On some aspects of fully-developed turbulent flow inrectangular channels. *Journal of Fluid Mechanics*, 23:689–713, 1965.

[5] E. Brundrett and W. D. Baines. The production and diffusion of vorticity in duct flow. *Journal of Fluid Mechanics*, 19(03):375–394, 1964.

[6] S. I. Hogg and B. E. Launder. Three dimensional turbulent corner wall jet. *Aeronautical Journal*, 89(885):167–171, 1985.

[7] H. Viets and P. M. Sforza. An experimental investigation of a turbulent, incompressible, three-dimensional wall jet. Technical Report 968, AFOSR, 1966.

[8] Nallamuthu Rajaratnam and Bidya S. Pani. Three-dimensional turbulent wall jets. *ASCE J Hydraul Div*, 100(HY1):69–83, 1974.

[9] B. E. Launder and W. Rodi. The turbulent wall jet - measurements and modeling. *Annual Review of Fluid Mechanics*, 15:429–459, 1983.

[10] V. P. Maslov, B. I. Minnev, A. N. Secundov, and A. N. Vorobiev. An experimental study of three-dimensional wall jets. *AIAA paper*, 2001. 2001-0449.

[11] J. W. Hall and D. Ewing. Three-dimensional turbulent wall jets issuing from moderate-aspect-ratio rectangular channels. *AIAA Journal*, 45(6):1177–1186, 2007.

[12] K. K. Adane and M. F. Tachie. Numerical investigation of three-dimensional laminar wall jet of newtonian and non-newtonian fluids. *AIAA Journal*, 46(11):2868–2880, 2008.

[13] J. W. Hall. The role of the large-scale structures in the development of turbulent wall jets. 2004.

[14] B. G. Newman, R. P. Patel, S. B. Savage, and H. K. Tjio. Three-dimensional wall jet originating from a circular orifice. *Aeronautical Quarterly*, 23:188–200, 1971.

[15] G. Padmanabham and B. H. L. Gowda. Mean and turbulence characteristics of a class of three-dimensional wall jets. part 1. mean flow characteristics. *Journal of Fluids Engineering, Transactions of the ASME*, 113(4):620–628, 1991.

[16] H Abrahamsson, B Johansson, and L Lofdahl. Turbulence field of a fully developed three-dimensional wall jet. Technical report, 1997.

[17] D. Sun, M. Ewing. Effect of initial and boundary conditions on the development of three-dimensional wall jet. *In the proceedings of the AIAA of the winter meeting, Tahoe*, 2002. AIAA 2002-0733.

[18] J. W. Hall and D. Ewing. Spectral linear stochastic estimation of the turbulent velocity in a square three-dimensional wall jet. *Journal of Fluids Engineering, Transactions of the ASME*, 132(5):0512031–0512039, 2010.

[19] J. W. Hall and D. Ewing. The asymmetry of the large-scale structures in turbulent three-dimensional wall jets exiting long rectangular channels. *Journal of Fluids Engineering, Transactions of the ASME*, 129(7):929–941, 2007.

[20] R. R. Schwab. *Three-dimensional jets formed using rectangular orifices.* PhD thesis, Queens University, Kingston, Ontario, CA, 1988.

[21] Sforza PM and Herbst G. Study of three-dimensional, incompressible, turbulent wall jets. *AIAA Journal*, 8(2):276–283, 1970.

[22] T. J. Craft and B. E. Launder. On the spreading mechanism of the three-dimensional turbulent wall jet. *Journal of Fluid Mechanics*, 435:305–326, 2001.

[23] Lhendup Namgyal and Joseph W. Hall. Piv measurements of the turbulent secondary flow in a three-dimensional wall jet. In *Proceedings of ASME 2010 3rd Joint US-European Fluids Engineering Summer Meeting and 8th International Conference on Nanochannels, Microchannels*, 2010.

[24] Lhendup Namgyal. *Three-component particle image velocimetry measurements in a turbulent three-dimensional wall jet.* PhD thesis, University of New Brunswick, Dept. of Mechanical Engineering, 2012.

[25] H.C. Essentials of fluid dynamics. by l. prandtl. london (blackie and son), 1952. pp. x, 452; many figures. 35s. *Quarterly Journal of the Royal Meteorological Society*, 79(342):570–570, 1953.

[26] M. Zamir and A.D. Young. Experimental investigation of boundary layer in a streamwise corner. *Aeronautical Quarterly*, 21:313–339, 1970.

[27] H. Xu. Direct numerical simulation of turbulence in a square annular duct. *Journal of Fluid Mechanics*, 621:23–57, 2009.

Curriculum Vitae

Candidate's full name:

Barrett James Poole.

University attended (with dates and degrees obtained):

University of New Brunswick 2009, Bachelor's of Science in Engineering.

Publications:

Poole, B.J., Hall, J.W., 2014, "Turbulence Measurements in the Corner Wall Jet. submitted to ASME/IMECHE Symposium on Fluid Measurements and Instrumentation, IMECE2014-38371. Submitted.

Conference Presentations: N/A.